Advance Temperature Modeling of Solar PV

Md Abdul Adud Shikder

A Thesis

In the Department

of

Electrical and Computer Engineering

Presented in Partial Fulfillment of the Requirements

for the Degree of Master of Applied Science at

Concordia University

Montreal, Quebec, Canada

November 2011

CONCORDIA UNIVERSITY
School of Graduate Studies

This is to certify that the thesis prepared

By: Md Abdul Adud Shikder

Entitled: Advance Temperature Modeling of Solar PV

and submitted in partial fulfillment of the requirements for the degree of

Master of Applied Science

complies with the regulations of the University and meets the accepted standards with respect to originality and quality.

Signed by the final examining committee:

Dr. Samar Abdi Chair

Dr. Andreas Athienitis Examiner

Dr. Pouya Valizadeh Examiner

Dr. Pragasen Pillay Supervisor

Approved by _____
Chair of Department or Graduate Program Director

_____
Dean of Faculty

Date _____

ABSTRACT

Advance Temperature Modeling of Solar PV

Md Abdul Adud Shikder

The low electrical efficiency of the mono-crystalline silicon photovoltaic module is a major drawback that reduces the competitiveness of solar photovoltaic power generation. The purpose of this thesis is to determine the improved efficiency by cooling of the mono-crystalline solar photovoltaic module with the prevailing winds in rural areas. The effect of the prevailing winds was determined by measuring the temperature of the mono-crystalline solar photovoltaic module using an advanced thermal model of the flat plate collector. The surface azimuth of the module is adjusted to minimize the angle between the prevailing wind and module surface to obtain optimum cooling for maximum output power. An analytical relationship between wind speed, wind direction, and panel surface azimuth is developed to achieve maximum output. It is observed in the thermal model that for a wind speed variance of 4 m/s, the efficiency of mono-crystalline silicon solar module increased by 22.9%. Experiments had been carried out in the Concordia solar simulator laboratory where 2.2% variation were found between calculated and experiment results for output power and efficiency. The experiment also validated the temperature variation in different solar cells within the module, which causes a loss in open circuit voltage and output power.

Acknowledgement

It is firstly due to the compassion and blessing of the almighty Allah (swt) has allowed me to complete my thesis.

I am extremely grateful and appreciate the efforts of my supervisor Prof. Pragasen Pillay, for his valuable direction, constructive suggestions, continuous patience & professional supervision throughout the course of my research.

I am also grateful to Prof. Andreas Athienitis and his PhD students Costa Kapsis and Yi Chao for their assistance while conducting the experiment in the state of art solar simulator laboratory at Concordia University.

Finally, my family deserves special thanks for displaying support and understanding during my study. It was my pleasure that my son Wasif helped me to proof read the thesis report.

Table of Contents

List of Figures

List of Tables

Nomenclature

Symbols

a	Constant for thermal model
A_C	Exposed area of collector, m^2
B	Breadth of solar panel, m
b	Constant for thermal model
c	Speed of light,
C_p	Specific heat of the air, J/(KgxK)
E	Energy of photon, eV
E_G	Band gap energy, eV
E_{G0}	Band gap energy, eV
F_g	Heat gain factor
g	Gravitational force, m/s^2
G_T	Incident heat energy, W/m^2
h	Heat transfer co-efficient, W/m^2K
h	Plank's constant,
H	Power density emitted from sun, W/m^2
H_{sun}	Power density at sun's surface, W/m^2
I_{dg}	Diffuse ground instantaneous irradiance, W/m^2
I_{ds}	Diffuse sky instantaneous irradiance, W/m^2
I_m	Current at maximum power, amps
I_o	Cell output current, amps

I_{on}	Extraterritorial solar radiation, W/m^2
I_s	Dark saturation current, amps
I_{sc}	Short circuit current, amps
I_{sc}	Solar constant, W/m^2
I_t	Total instantaneous irradiance, W/m^2
I_λ	Light generated current, amps
k	Boltzmann constant, $1.38x10^{-23}$ joules/K
k	Thermal conductivity, W/mK
L	Latitude, degree
m	Fluid mass flow rate
n	Day of the year
n	Ideality factor
N_A	Doping concentration, cm^{-3}
n_i	Intrinsic carrier concentration, cm^{-3}
Nu	Nusselt number,
P_{in}	Input power, watts
P_{max}	Maximum power, watts
q	Electric charge (elementary charge), $1.6x10^{-19}$ Coulombs
Q_u	Total heat recovered in collector, W
R1	Thermal resistance, m^2K/W
R2	Thermal resistance, m^2K/W
R3	Thermal resistance, m^2K/W
R4	Thermal resistance, m^2K/W

R5	Thermal resistance, m^2K/W
Ra	Rayleigh number
R_{base}	Resistance of base, ohms
R_{busbar}	Resistance of busbar, ohms
R_{CH}	Characteristics resistance, ohms
Re	Reynold number
$R_{emitter}$	Resistance of emitter, ohms
R_{finger}	Resistance of finger, ohms
R_p	Shunt resistance, ohms
R_s	Series resistance, ohms
R_{sun}	Radius of sun, m
T	Temperature, K
T_a	Ambient temperature, K
T_c	Cell temperature, K
T_m	Module temperature, K
T_p	Flat plate collector temperature, K
U_b	Bottom heat loss co-efficient, W/m^2K
U_e	Edge heat loss co-efficient, W/m^2K
U_t	Top heat loss co-efficient, W/m^2K
V	Output voltage of cell, volts
V_{G0}	Open circuit voltage at absolute zero, volts
V_m	Voltage at maximum power, volts
V_{oc}	Open circuit voltage, volts

$V_{OC'}$	Normalized voltage, volts
W1	Coefficient for temperature
W2	Coefficient for irradiance, $^0C/W.m^{-2}$
W3	Coefficient for wind speed, $^0C/m.s^{-1}$
W4	Coefficient for wind direction, $^0C/deg$
W5	Coefficient for humidity, $^0C/RH\%$

Abbreviation

AM	Air Mass
BIPV	Building integrated photovoltaic
EVA	Ethyl vinyl acetate
FF	Fill factor
NOCT	Nominal operating cell temperature
STC	Standard testing condition

Greek letters

α	Solar altitude, degree
β	Tilt angle, degree
β'	Volumetric co-efficient
γ	Solar surface azimuth, degree
δ	Declination angle, degree
Δn	Excess carrier concentration, cm^{-3}
ΔX	Thickness, m
ε	Emissivity
η	Efficiency

θ_z	Zenith angle, degree
λ	Wavelength of light, μm
ρ	Diffuse ground reflectance
τ	Solar transmittance
τ_b	Beam transmittance
τ_d	Diffuse transmittance
Φ	Photon flux, $m^{-2}s^{-1}$
φ	Solar azimuth angle, degree
ψ	Surface azimuth, degree

Chapter 1 : Introduction

1.1 Global Energy Analysis

By 2035, the world energy consumption is projected to increase by roughly 49% from year 2007 [1]. This prediction is based on the projected consumption in Figure 1.1 which indicates the worldwide trend of energy demand since 1990 and provides projections of energy consumption to 2035 based on previous growth patterns and other factors [1].

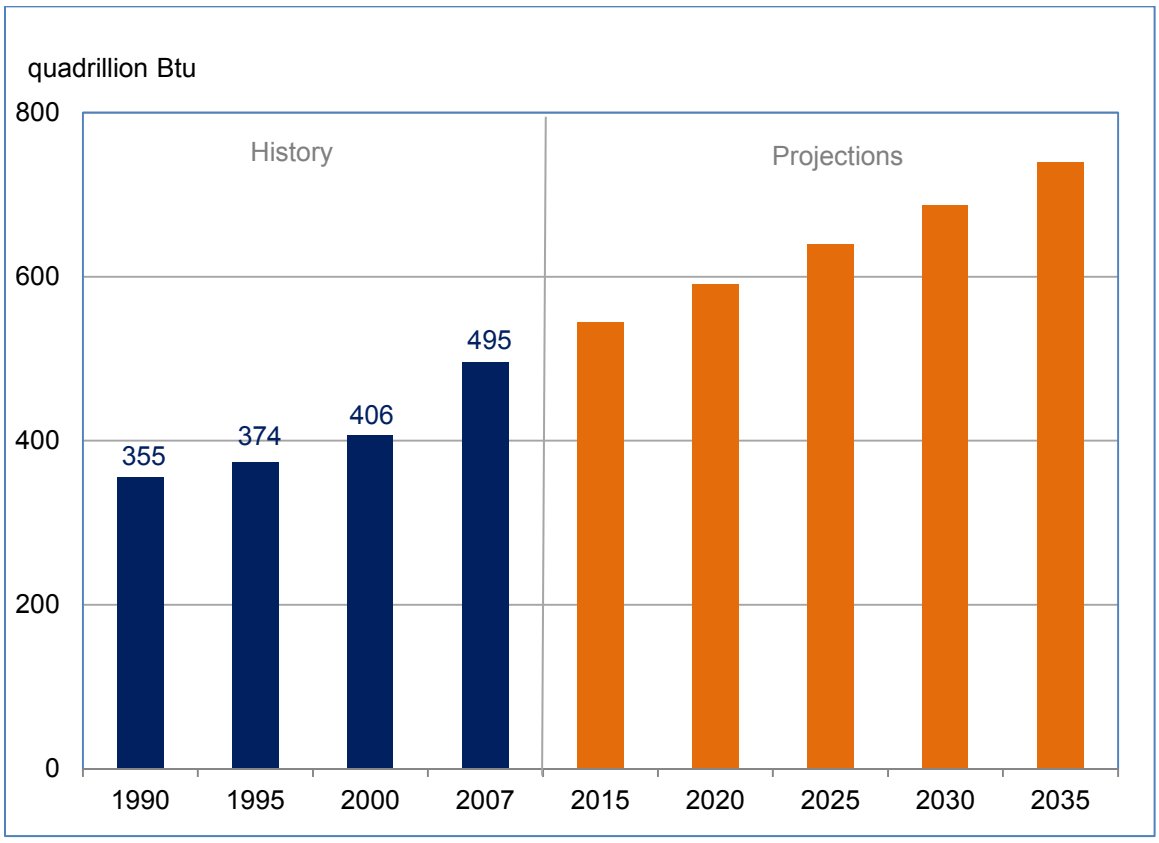

Figure 1.1: "World Marketed Energy Consumption, 1990-2035. [1]"

Figure 1.2 illustrates the global energy use by fuel type. Fossil fuels have been targeted to reduce from 85% in the year 2007 to 80% in the year 2035. Renewable energy has an expected growth from 10% to 14% during the same period.

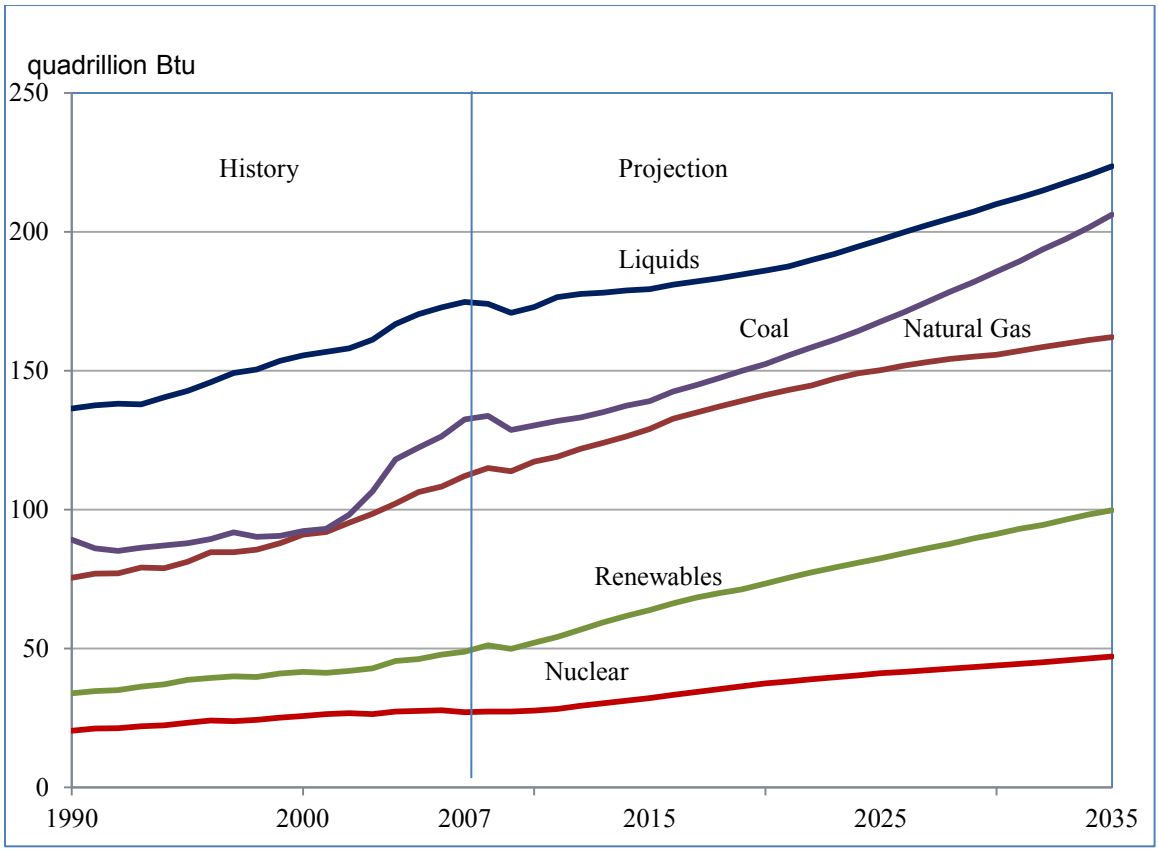

Figure 1.2: "World Marketed Energy Use by Fuel Type, 1990-2035. [1]"

It is well-known that fossil fuels are unequally concentrated in areas around the world, which may cause future tensions between countries if their economy is exceedingly reliant on these scarce resources. Furthermore, producing and utilizing electrical energy by using the present day technologies has caused substantial damage to the Ozone layer and the environment of many areas around the world. As a result, it is an important task for humanity to discover a way to create the required amount of energy, while using the most efficient sources. The generation of electricity is expected to increase by nearly 87% by 2035, as shown in Figure 1.3. The U.S. is responsible for the utilization of almost 21% of the total global electricity demand, and is expected to rapidly fall approximately to 16% by the year 2035. The electrical requirements will be lead by the developing economies of China and India 30% by 2035. In 2007 both of these countries used only

20% of the world's requirement. In order to support the required electrical demands of the future, a widespread extension of production power is essential. Global production power is anticipated to increase from 18.77 trillion kWh in 2007 to about 35.17 trillion kWh in 2035 (Figure 1.3) with an average yearly growth rate of 2.3%.

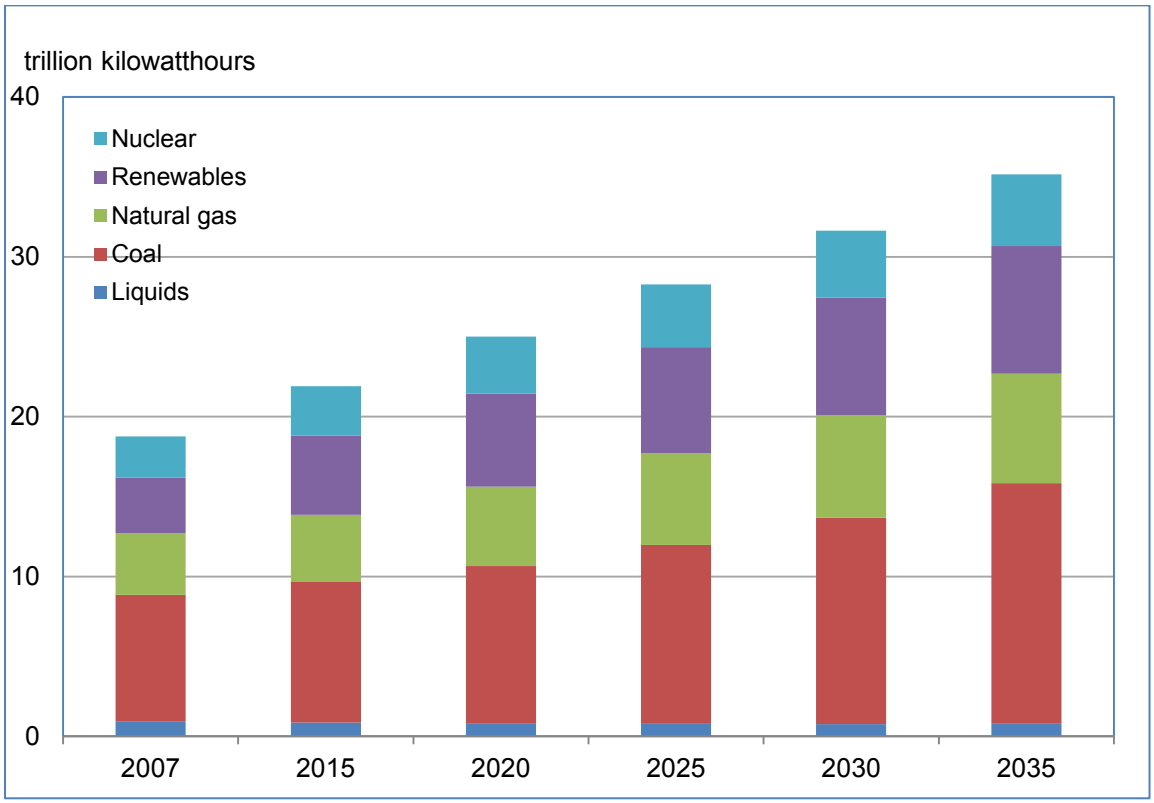

Figure 1.3 : "World Electricity Generation by Fuel, 2007-2035. [1]"

Currently electricity is produced from fossil fuels, nuclear energy, renewable sources and other generating units. In 2007 fossil fuels (mainly consisting of coal, natural gas and liquids) and nuclear plants were responsible for 90% of the total production. 3% annual growth was observed in renewable energy, where hydroelectric and wind power experienced remarkable growth. In international annual energy outlook 2010 report, renewable electricity generation is projected as per Table1.1. In the case of solar energy the highest average annual percent change (12.7%) has been predicted.

Table 1.1: "World net renewable electricity generation by energy source, 2007-2035 (billion kWh). [1]"

	2007	2015	2020	2025	2030	2035	% change 2007-2035
Hydropower	2,999	3,689	4,166	4,591	5,034	5,418	2.1
Wind	165	682	902	1,115	1,234	1,355	7.8
Geothermal	57	98	108	119	142	160	3.7
Solar	6	95	126	140	153	165	12.7
Other	235	394	515	653	773	874	4.8
Total World	**3,462**	**4,958**	**5,817**	**6,618**	**7,336**	**7,972**	**3.0**

1.2 Role of Photovoltaic in Renewable Energy

Energy from the sun naturally powers the weather, affecting the temperature that causes the water and wind cycles. The sun provides energy to living organisms: plants generate energy from the sun's rays through photosynthesis and a smaller amount of energy is transmitted from the plant to other living organisms through consumption. The innovation in technology provides society with the ability to capture and utilize solar energy to fulfill increasing energy demands.

1.3 Motivation and Contribution of the Research

The harnessing of power from various natural resources and the sun has evolved into a prominent research area. At the onset of the 1960's, researchers developed innovative technologies for power generation by harnessing sunlight through photovoltaic devices. Solar technology has not been commercialized globally due to high cost and low electrical efficiency.

In a particular region, prevailing winds flowing from a specific direction are responsible for cooling in that area. The solar panels are normally positioned at a tilt angle based on the latitude of the region and independent of wind direction. The prevailing winds are responsible for cooling of the photovoltaic cells and the temperature of the panel varies with the azimuth and tilt angle. This thesis investigates the correlation between the module efficiency, module output power and the temperature of the panel due to the cooling by the prevailing winds.

1.4 Overview of the Thesis

In chapter 2 photovoltaic fundamentals, solar cell operation, modules, arrays and PV systems are discussed.

Chapter 3 is entitled "Comparison of Software for the Determination of Output Power Based on Seasons". Various available PV software packages are analyzed and their features are highlighted. The importance of software in designing the PV installation considering weather and shading in urban areas has been studied. A case study in an urban area of Montreal is simulated for software comparison.

The cooling effect by prevailing winds on the solar panel is discussed in chapter 4. A thermal model is developed to achieve optimum power, considering cooling from prevailing wind speed and direction. Experimental data is compared with the simulated data for model accuracy.

Mismatch in solar cell characteristics affect the short circuit current and open circuit voltage. This mismatch causes the temperature variation in solar cells in the PV panel. Changes in efficiency and output power due to variation of temperatures in different cells are modeled in chapter 5.

Future work mentioned in chapter 6.

Chapter 2 : Photovoltaic Fundamentals

2.1 Introduction

In the photovoltaic (PV) process, sunlight is converted into electrical energy through solar cells. Photovoltaic power conversion is reliable with no moving components. Operation and maintenance costs of such systems are very low compared to other electricity generating systems. The operation of photovoltaic systems is silent and environmentally friendly as it does not emit carbon dioxide into the atmosphere. The module can be installed quickly and produces standalone or grid connected electricity.

2.2 Solar Energy

Solar energy is radiant ultraviolet light and heat from the sun and it is converted into wind, wave power, hydro electricity and biomass. A portion of this vast renewable energy source available on earth is directly used by humans. Earth receives $174x10^{15}$ Watts at the extraterritorial level: 30% is reflected back to space, and 70% is absorbed by clouds, water and land masses [2]. Chemical energy is achieved from solar energy through photosynthesis which produces food, wood, biomass etc. Finally fossil fuels are available from these products. Table 2.1 describes the comparison between incoming solar energy and human energy consumption.

Table 2.1 : "Yearly Solar Fluxes and Human Energy Consumption."

Solar Energy	$3850000x10^{18}$ Joules [3]
Wind Energy	$2250x10^{18}$ Joules [4]
Biomass Energy	$3000x10^{18}$ Joules [5]

Primary energy use (2006)	497.5×10^{18} Joules [6]
Electricity (2006)	58.9×10^{18} Joules [7]

2.3 Properties of Sunlight

Sunlight is a form of electromagnetic radiation and visible light is a part of the electromagnetic spectrum. The sun emits X-rays, ultraviolet, visible light, infrared and radio waves, where ultraviolet rays are not absorbed by atmosphere and cause sunburn to human body. Considering wavelengths, sunlight can be divided into five groups namely Ultraviolet C (100-280 nm), Ultraviolet B (280-315 nm), Ultraviolet A (315-400 nm), visible light (380-780 nm) and infrared (700 nm – 1 mm)[8].

Plank and Einstein described light as a photon which consists of wave packet or particle of energy.

2.3.1 Energy of a Photon

The photon can be defined as massless, no electric charge and does not decay in free space. It has linear and circular polarization, also characterised by it's wave vector components and direction of propagation. The energy of the photon E, expressed by equation, $E = \frac{hc}{\lambda}$, where h=Plank's constant, c=speed of light and λ=wavelength of light. This equation explains that the lower wavelength photon (blue light) has higher energy and the higher wavelength photon (red light) has lower energy. In the case of photon, the energy unit is used as electron Volt (eV) instead of joules. Photon energy is commonly expressed in electron-volt and wavelength as follows,

$$E = \frac{1.24}{\lambda(\mu m)}\ eV \tag{2.1}$$

Photon flux is expressed as the number of photons in unit time and unit area and defined in equation 2.2.

$$\Phi = \frac{no.of\ photons}{sec\ X\ m^2} \tag{2.2}$$

The power density is calculated by multiplying photon flux and photon energy. If the power is expressed in W/m^2, then the energy of photon should be in joules as follows [9].

$$H = q\Phi \frac{1.24}{\lambda(\mu m)} (\mathrm{W/m^2}) \tag{2.3}$$

2.3.2 Sun's Temperature

In sun's core hydrogen is converted to helium due to nuclear fusion at a temperature of 20 million degrees Kelvin. The sun's surface is layered with hydrogen where heat transfer occurs through convection; hence no radiation is visible from the inner core. The photosphere, the surface of the sun, has a temperature of 5762±50K and 5730±90K [10]. Total energy emitted from surface of the sun is 9.5x10^{25} W [11].

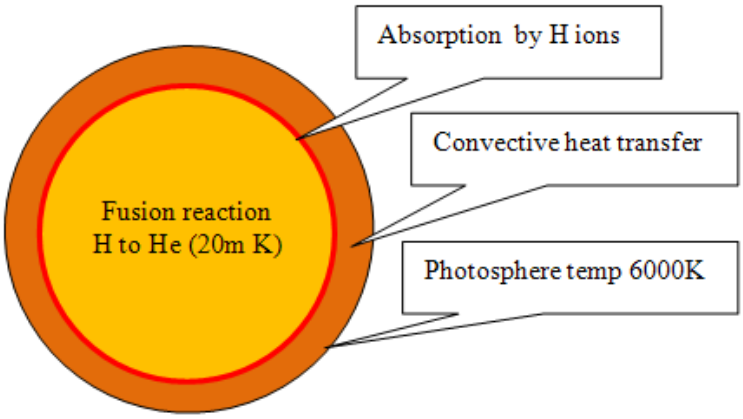

Figure 2.1 : "Sun's Temperature. [12]"

2.3.3 Solar Radiation

Total power impinges on an object in space is a fraction of sun's emitted power. At sun's surface total power will be the blackbody power density multiplied by sun's total surface area. If R_{sun} is the radius of the sun, total energy radiated from the sun is $\sigma T^4 x 4\pi R_{sun}^2$, where σ is the Stephen Boltzmann constant. At a distance D, this energy will be illuminated over an area of $4\pi D^2$. Hence solar radiation intensity H_0 at an object at a distance D will be as follows.

$$H_0 = \frac{R_{sun}^2}{D^2} H_{sun} \tag{2.4}$$

Where R_{sun} is the radius of the sun, H_{sun} is the power density (W/m^2) at sun's surface and D is the distance as figure 2.2.

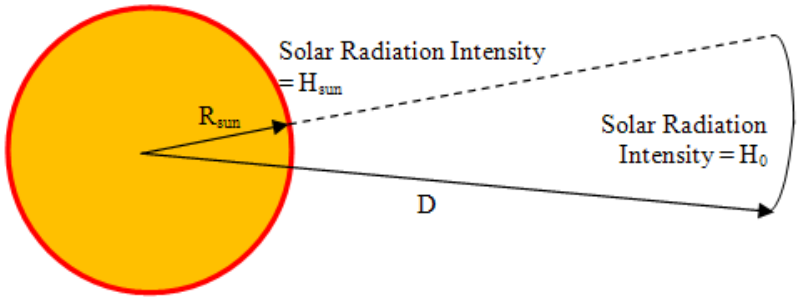

Figure 2.2 : "Solar Radiation Intensity Reduced at a Distance. [13]"

2.3.4 Solar Geometry for PV Panel

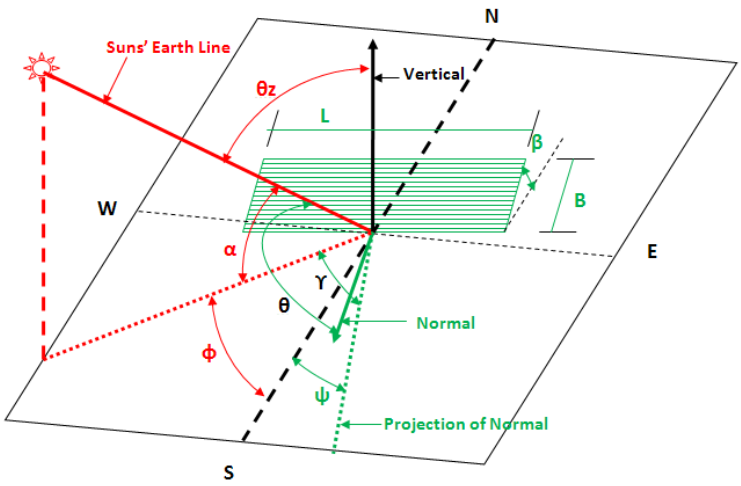

Figure 2.3 : "Solar Geometry for PV Panel. [14]"

Declination angle (δ) is the angle between equator of the earth and a line between centre's of the earth and sun. Declination angle varies between -23.45^0 to $+23.45^0$ during the year.

Azimuth angle (φ) is the compass direction of the sun. In general, azimuth angle varies with time of the day, latitude and day of the year.

Solar angle (α) is the angular height of the sun from horizontal.

Zenith angle (θ_z) is the complementary of the solar angle.

2.3.5 Solar Equations

The following solar equations are used in this thesis to find out solar time, local time, solar angles etc. [15]

Local standard time meridian $LSTM=15^0\Delta T_{GMT}$ (2.5)

Equation of Time, $EoT = 9.87 \sin 2B - 7.53 \cos B - 1.5 \sin B$ (2.6)

Where $B = \frac{360}{365}(n - 81)$

Time correction factor, $TC = 4(L - LSTM) + EoT$ (2.7)

Local solar time, $LST = LT + \frac{TC}{60}$ (2.8)

Hour angle, $\omega = 15^0(LST - 12)$ (2.9)

Declination angle, $\delta = 23.45^0 \sin\left[\frac{360}{365}(n - 81)\right]$ (2.10)

Solar altitude, $\alpha = \sin^{-1}[\sin\delta \sin L + \cos\delta \cos L \cos\omega]$ (2.11)

Solar azimuth, $\varphi = \cos^{-1}\left[\frac{\sin\delta \cos L - \cos\delta \sin L \cos\omega}{\cos\alpha}\right]$ (2.12)

2.4 PN Junction

When a junction between a p type and n type semiconductor material is formed, holes and electrons diffuse from a higher concentration to a lower concentration surface separated by the junction. The remaining ionized impurities that are left after the recombination of holes and electrons accumulate in the form of a layer along the junction which is known as depletion layer. The positively-charged ionized impurities form the positively charged layer while negatively-charged ionized impurities form the negatively charged layer, which results in an electrostatic potential along the junction which causes an electric field in the depletion region.

This voltage difference produces an energy barrier that further hinders the recombination of an electron-hole pair from the opposite sides of the junction and thus stops the flow of charge. This energy barrier is known as potential energy hill, energy gap or barrier voltage. A detailed diagram is given in the figure 2.4.

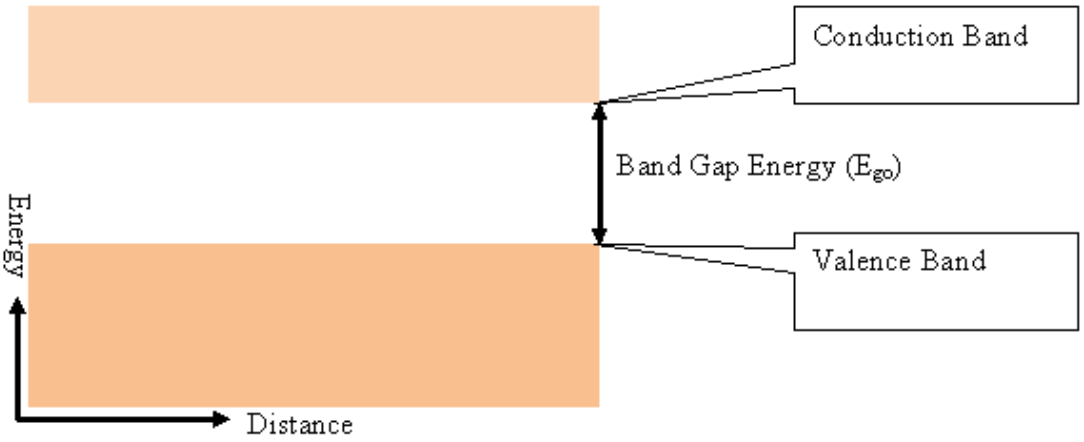

Figure 2.4 : "Schematic of Band Energy For electrons. [16]"

2.5 Solar Cell Operation

The solar cell is an electronic device which directly converts solar energy into electricity. The solar cell produces electrical voltage and current to produce electrical power from incident sunlight. Photons excite electrons in the solar cell to move to a higher energy state and then electrons transfer this energy to an external circuit. Finally this electron returns to the solar cell and in the industry this energy conversion process occurs through semiconductors in the form of a p-n junction.

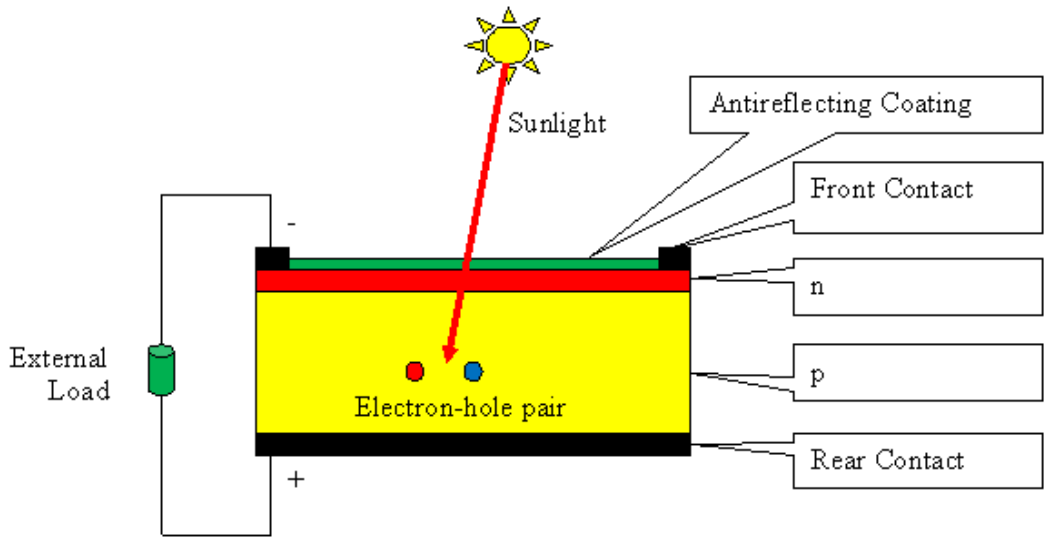

Figure 2.5 : "Solar Cell Cross Section. [17]"

Operation of solar cell can be divided into four phases, generation of light-generated carriers; these carriers generate a current; a large voltage develops across the solar cell; and finally power dissipates in the load and parasitic resistance [17].

2.5.1 I-V Curve

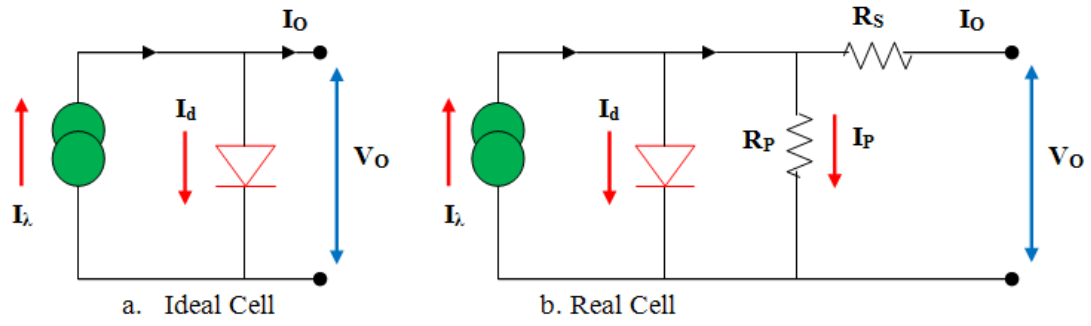

Figure 2.6 : "Equivalent Circuit of Ideal and Real Cells. [18]"

The solar cell is represented in an electrical circuit as a current source with a parallel diode. When sunlight is incident on the solar cell, it starts producing current which passes through the diode and external loads. In a real cell, two types of internal resistances exist. As the sunlight intensity increases, the light generated current also increases in the cell. A detailed schematic is given in figure 2.6 for ideal and real solar cells.

The equations of ideal and real solar cells are provided below [19].

For the ideal cell, $I_o = I_\lambda - I_S\left(e^{\frac{qVo}{kT}} - 1\right)$ (2.13)

For a real cell, $I_o = I_\lambda - I_S\left(e^{\frac{q(Vo+I_oR_S)}{nkT}} - 1\right) - \frac{Vo+I_oR_S}{R_P}$ (2.14)

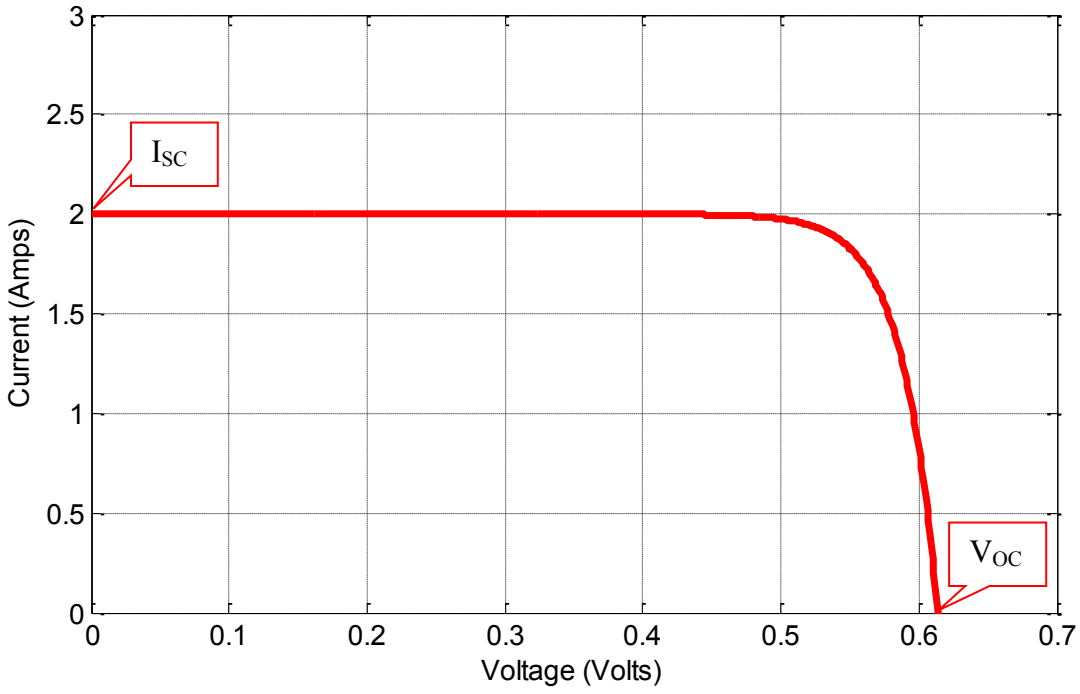

Figure 2.7 : "I-V Curve for a Ideal Silicon Cell. [20]"

2.5.2 Short Circuit Current (I_{SC})

The short circuit current is the maximum current through the solar cell and occurs when the voltage across the cell is zero. Normally the short circuit current depends on incident solar radiation, cell area, optical properties, collection probability etc. Under 1.5 airmass (AM) spectrum the theoretical current density for a silicon solar cell is 46 mA/cm^2. In the laboratory 42 mA/cm^2 current has been measured whereas commercial silicon cell short circuit currents are between 28 mA/cm^2 to 35 mA/cm^2 [21].

2.5.3 Open Circuit Voltage (V_{OC})

The open circuit voltage is the maximum voltage available across the solar cell with zero output current. The equation for open circuit voltage is given in equation

$$V_{OC} = \frac{nkT}{q} \ln \frac{I_\lambda + I_S}{I_S} \tag{2.15}$$

So, from the above equation it is clear that the open circuit voltage depends on dark saturation current. This dark saturation current is mainly dependent on recombination in the solar cell. Open circuit voltage also expressed in carrier concentration as follows [22].

$$V_{OC} = \frac{kT}{q} \ln \left[\frac{(N_A + \Delta n)\Delta n}{n_i^2} \right] \tag{2.16}$$

Where kT/q is the thermal voltage, N_A is the doping concentration, Δn is the excess carrier concentration n_i is the intrinsic carrier concentration.

2.5.4 Fill Factor (FF)

Fill factor is the ratio of maximum power (P_{max}) to the theoretical power limit (V_{OC}xI_{SC}) of the solar cell and expressed as follows.

$$Fill\ Factor\ (FF) = \frac{V_m I_m}{V_{OC} I_{SC}} \tag{2.17}$$

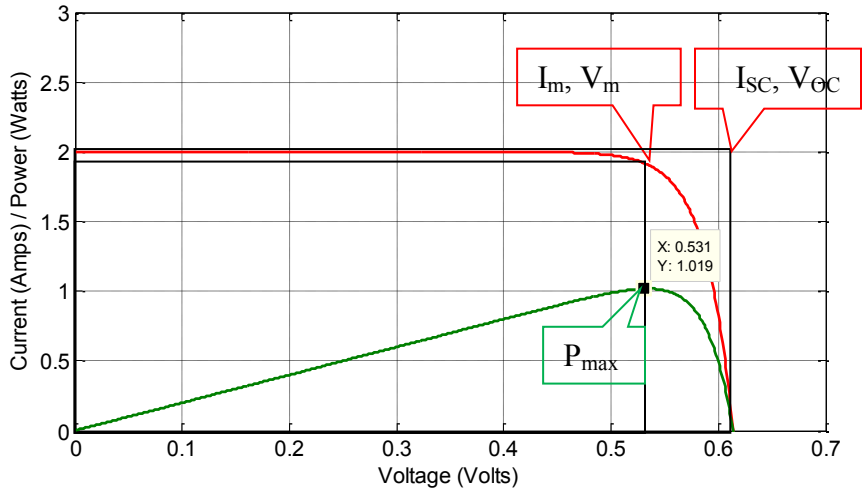

Figure 2.8 : Fill Factor and Maximum Power Curve for a Ideal Silicon Cell

FF also indicates the squareness of the I-V curve. Higher voltage provides lower squareness of the I-V curve and fill factor. Maximum fill factor can be achieved by differentiating the solar cell power with respect to voltage.

$$V_m = V_{OC} - \frac{nkT}{q} \ln\left(\frac{V_m}{\frac{nkT}{q}} + 1\right) \tag{2.17}$$

Where Vm is the voltage at maximum power and n is the ideality factor.

Equation 2.17 does not provide values of V_m and V_{OC} but only relates them, further I_{SC} and FF also unknown. Following empirical equation is widely used for FF [23].

$$FF = \frac{V_{OC\prime} - \ln(V_{OC\prime} + 0.72)}{V_{OC\prime} + 1} \text{ (where } V_{OC\prime} = \frac{q}{nkT} V_{OC}) \tag{2.18}$$

2.5.5 Efficiency

The efficiency of the solar cell is measured by the ratio of solar cell output energy to

incident sun energy. The efficiency depends on the spectrum and the intensity of sunlight and solar cell temperature. To compare one solar cell to another 1.5 AM (air mass) condition and 25^0 C temperatures are maintained. The equation for solar cell efficiency is given below [24].

$$\eta = \frac{V_{OC} I_{SC} FF}{P_{in}} \tag{2.19}$$

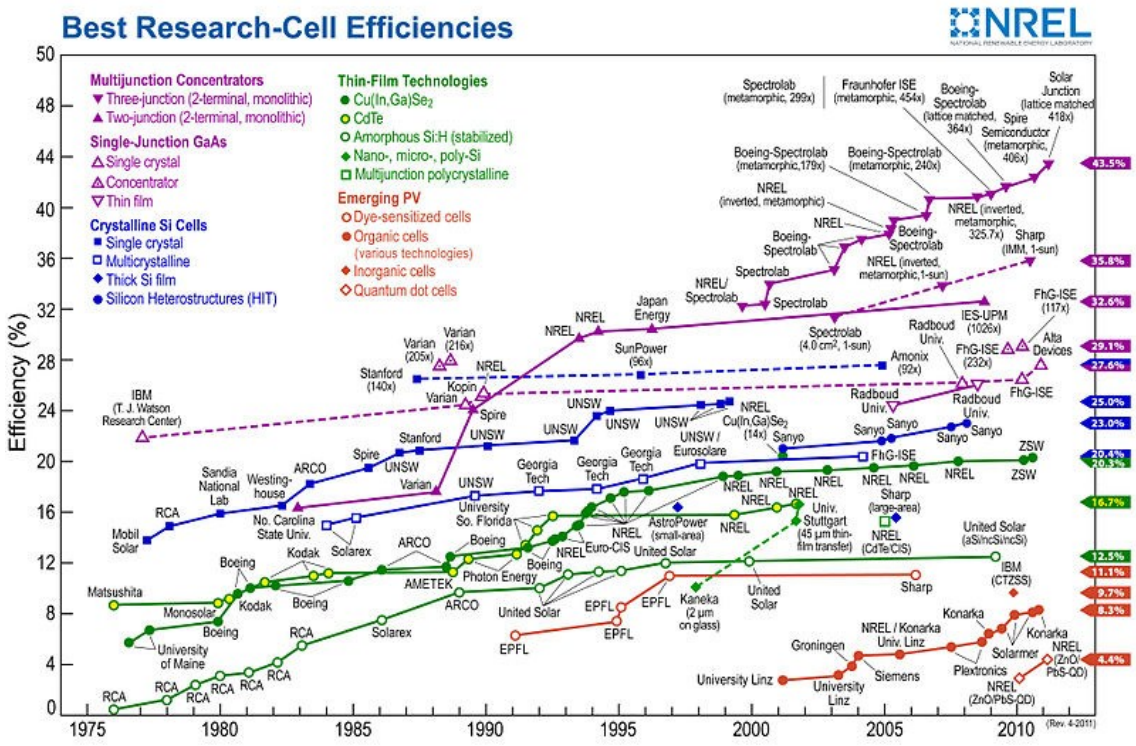

Figure 2.9 : "Chart for Laboratory Efficiency of Various Solar Cells. [25]"

Conversion efficiencies of the best research solar cells from 1976 to 2011 are indicated in figure 2.9. These efficiencies were determined by certified agencies or laboratories.

2.5.6 Resistances

Characteristic resistance is the output resistance for maximum power and is expressed as follows.

$$R_{CH} = \frac{V_m}{I_m} \tag{2.20}$$

If the load has this resistance, then the solar cell delivers maximum power to the load.

There are two types of parasitic resistances in the solar cell, a series resistance and a shunt resistance. The efficiency of the cell reduces due to power losses in the parasitic resistances.

The series resistance is mainly due to design imperfections of the solar cell. This resistance reduces the short circuit current of the cell. A typical value for laboratory type silicon solar cell is 0.5 Ωcm^2 and a commercial one is up to 1.3 Ωcm^2 [26].

The shunt resistance provides an alternate path for current to flow and reduces the open circuit voltage of the solar cell. Shunt resistances are the effect of manufacturing fault of the solar cell. Typical values of shunt resistances are $M\Omega cm^2$ for laboratory cells, and 1000 Ωcm^2 for commercial cells.

2.6 Solar Cell Materials and Generations

Solar cells are mainly produced from silicon based materials, although there are some other materials emerging in the industry. Research is on going to improve efficiency and lower the cost of materials. Existing commercial and laboratory solar cell materials are as follows [27].

Crystalline Silicon	Mono-crystalline Silicon (c-Si)
	Poly or multi-crystalline silicon (poly-Si or mc-Si)
Thin Films	Cadmium telluride
	Copper indium gallium selenide
	Gallium arsenide multi-junction
	Light-absorbing dyes (DSSC)
	Organic/polymer
	Silicon thin films
	- Amorphous silicon (a-Si)
	- Proto-crystalline silicon
	- Nano-crystalline Silicon (nc-Si)

First generation solar cells are silicon and germanium based with phosphorous and boron dope in p-n junction. Second generation solar cells are amorphous silicon cells, polycrystalline silicon cells, copper indium di selenide cells etc. Researchers are trying to commercialize the third generation solar cells which will overcome the Shockley-Queisser efficiency limit [28]. Third generation tandem solar cells are made of amorphous silicon and gallium arsenide materials. In general p-n junction semiconductors solar cells are referred to as first generation and thin film solar cells are referred to second generation solar cells. The main goal of third generation solar cells is not only to compete against existing solar cells but also fossil fuels and nuclear energy.

2.7 Design of Silicon Cells

The objective of designing a silicon solar cell is to maximize efficiency. In theory photovoltaic conversion is 86.8% where only analytical calculation was done but no

practical device was considered. In a silicon cell the most realistic efficiency is 29% and till now 24.7% measured under 1.5 AM. Theoretical analysis considers all incoming photons are converted and assumes a high concentration ratio.

The principles of designing single junction solar cell are maximizing collection of photons, increasing carrier collection by p-n junction, minimizing forward bias dark current and reducing resistive losses. Optical losses occur due to reflection of light from different places of solar cell.

2.8 Modules and Arrays

The solar module is made of individually connected solar cells to increase the output power. This also protects internal parts from the environment and other electrical hazards for longevity. At the same time there are some issues raised due to interconnection and encapsulation of the solar cells, namely mismatch losses, module temperature variation, module lifetime etc. The typical warranty of a module ensures that it will produce output power up to 90% for the first 10 years and 80% up to 25 years of rated values. Third party insurance assures the guarantee in case of manufacturers' bankruptcy. The structure of a typical silicon solar PV module is shown in the figure 2.13 [29].

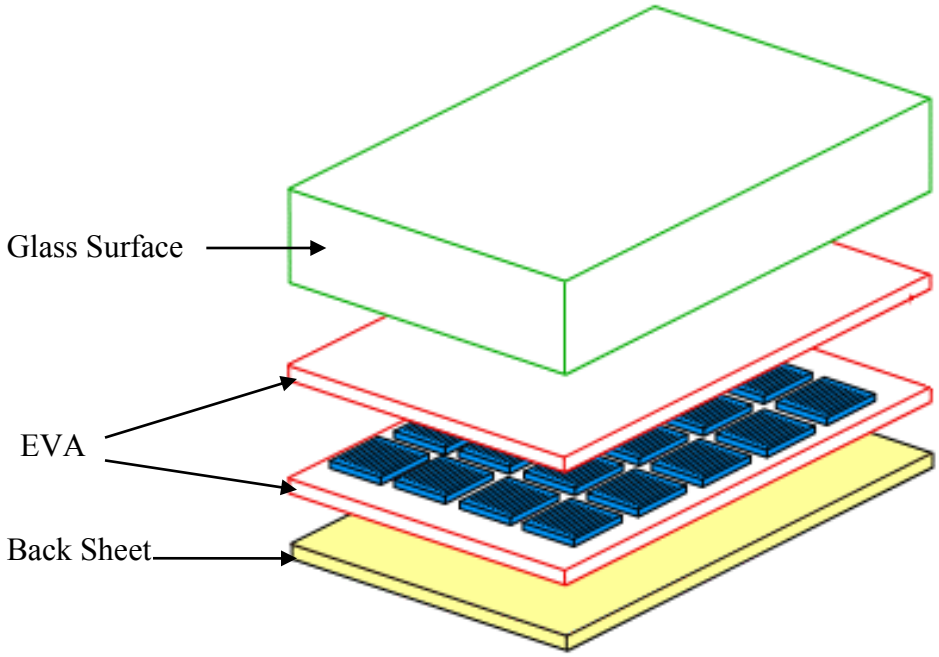

Figure 2.10 : "Structure of Silicon Solar PV Module. [29]"

One solar module is not enough to produce the required power for a household or business in a rural area. Hence modules are connected in series to produce operating DC voltage and thereafter sets of module are connected to reach the expected current.

2.9 PV Systems

In rural areas, where power grid is not available, stand-alone PV systems are popular and economical. DC power generated from PV systems directly feed the load through an inverter and charge the battery bank by charge controller for night use. In case of a fully charged battery, a dump load is used to consume the extra power. Diode D_B protects battery bank for overcharging and D_P restricts current flow from battery to panel during the nighttime.

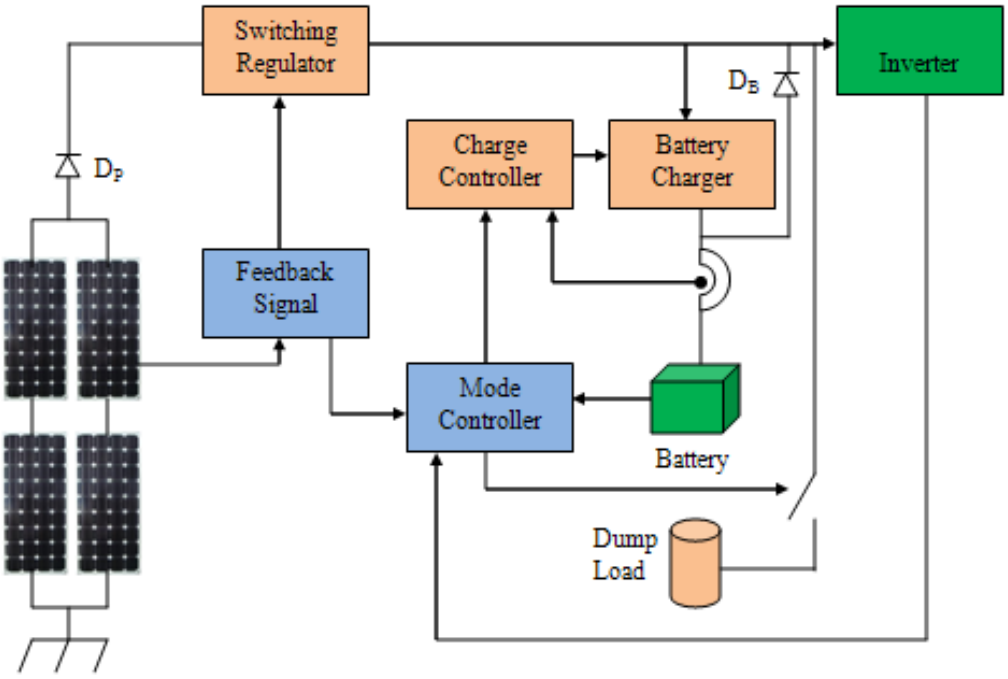

Figure 2.11 : "Standard Stand-alone PV Systems. [30]"

2.10 Conclusions

Fundamentals of solar energy conversion, design of silicon solar cell, efficiency of solar cell etc. are discussed in this chapter. Some basic concepts of solar modules and systems were also discussed.

Chapter 3 : Comparison of Softwares for Determination of Output Power Based on Seasons

Recently, the demand for renewable energy sources and the declining manufacturing costs of photovoltaic panels have increased the popularity of Building Integrated Photovoltaic (BIPV) Systems. There are many concerns regarding the appropriate design for different buildings, particularly in metropolitan conditions.

This chapter considers the issues regarding urban design and demonstrates a PV system design for a metropolitan commercial building in downtown Montreal. Insolation and shadow analysis were performed and analysis of different design scenarios was conducted. In addition, energy production levels of each scenario were measured and for the best scenario, the load energy demand is compared with the PV energy production level.

The use of PV systems in Canada has grown significantly from 2008 to 2009. The total electrical energy generated in 2008 through PV systems was 32.72 MW, the PV generation increased to 94.57 MW in 2009. The grid connected systems have experienced significant growth, they contributed 82.27 MW in 2009, whereas only 10.9 MW was in 2008. The major factor that influenced the growth of the PV systems was FiT (Feed in Tarrifs) program in Ontario, which was launched in 2006 and expanded in 2009 [31].

Currently, there are various software packages available in the market to simulate the project and measure PV output electrical power and other parameters for renewable energy. Some of these software packages are suitable for use in urban applications, whereas the others are more practical for use in rural areas.

In this thesis a study was made on appropriate application of software for solar power production in a building in downtown Montreal. Simulation was done in HOMER, PVSYST and ECOTECT software with two different sets of PV panels from different manufacturers. Results are discussed in detail with graphs and a recommendation is made accordingly.

3.1 Available Software in the Market

There are various software packages available in the market for planning, designing, monitoring and maintaining PV systems [32] [33]. Selection of the software mainly depends on user's requirement and available resources. HOMER, PVSYST and ECOTECT were selected for the case study and a brief description of them is provided as follows.

3.1.1 HOMER

HOMER is an energy modeling software that designs and performs analysis for hybrid power systems, consisting of conventional generators, cogeneration, wind turbines, solar photovoltaic, hydropower, batteries, fuel cells, biomass, and other inputs [34]. It is one of the most consistently used software with abundant applications. Homer integrates variable scenarios such as wind and solar into hybrid systems for grid-tied or off-grid environments.

HOMER has an abundance of applications in engineering and other fields of study. It can be used to simulate different energy systems to obtain results and a realistic estimate of their capital and operating expenses. HOMER also measures the economic expediency of a hybrid energy system, determines the optimal system design and educates the user about the process in which hybrid renewable systems operate.

Distributed generation and renewable power projects are sectors of the industry that continue to expand at an accelerated pace. HOMER allows utilities, system integrators and project developers in other fields to examine the financial risk of their hybrid projects. HOMER Energy consists of software, services, and an on-line community for the users designing hybrid systems.

3.1.2 PV SYST

PV SYST supplies the user the PV component sizes, determines the monthly production and conducts a preliminary economic evaluation of the PV system [35]. The project design component of the application conducts detailed simulation in hourly intervals, assists the user in defining the PV field and determines the appropriate components. These components provide the user with a report consisting of parameters and main results.

PV SYST consists of tools that conduct meteorological database and component management. The 3-D CAD Tool provides the user with the ability to illustrate the complete system with geometry. It measures the shading factor for the beam component as a function of the suns position. The shading for the diffuse radiation is considered using an integral of the shading factor over the sky portion observed by the array. The array can be partitioned to determine the electric losses caused by the string layout. The shading impact of a particular scenario is confirmed by the animation of a complete day.

3.1.3 ECOTECT

Ecotect is a building analysis tool that conducts simulation and analysis functions [36]. It consists of thermal and acoustic functions that must be provided with information about

adjacent zones to determine heat and sound flow. It is good sustainable building design software to conduct whole-building energy analysis, thermal performance, water usage and cost evaluation, solar radiation, day lighting, shadow and reflections etc.

3.2 Review of Previous Works

Siraki et al. used different software to design PV system in urban areas and also compared the results obtained from the software [37]. Attia et al. has developed a software (EGYPV Estimator v.1.0b) based on visual basic and mainly focused on architectural planning of the net zero energy building [38].

3.3 Case Study

Meteorological data, building design, surrounding shading objects and other input information were equal in all of the software. In the study, the first case, rooftop and façade PV panels were specified from Canadian Solar products. All panels on the roof have a tilt angle of 45^0. These panels are not used only as a source of electricity but also used as building construction materials. Newedge CS6P-235PX PV panels have been used in the simulation with dimensions of 1638x982x40mm and an output of 235 watts [39]. For the second case study, 20 sets of 13 m^2 Sharp NU-185W PV arrays were considered for simulation [40]. Each array consists of 10 PV panels with a dimension of 5000x2600mm. Ingecon Sun 3.68 TL inverters are used in the models with their standard efficiency and other technical parameters [41].

Latitude and longitude of Montreal is 45.4^0 N and 73.4^0 W respectively, hence the tilt angle of PV panel is considered as 45^0 for rooftop panels. Albedo for the site has been considered 0.2 in all simulations, whereas solar collector surface azimuth is considered

0^0. Shading objects dimensions and positions are acquired using Navigatuer Urban software of Montreal [42].

Figure 3.1: Neighborhood in Navigatuer Urban

In the ECOTECT software, either the 3D design can be drawn directly or can be imported from other CAD software. But PV SYST software does not allow importing CAD drawings from other software. PV SYST CAD is simpler to use than ECOTECT and is more customized for PV applications.

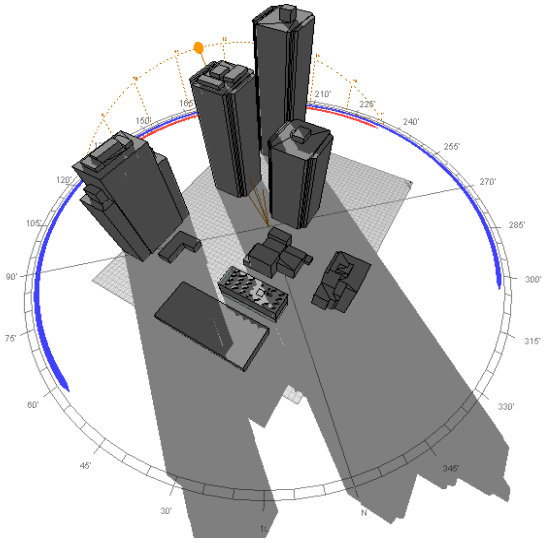

Figure 3.2 : 3D Model of the Project Site in ECOTECT

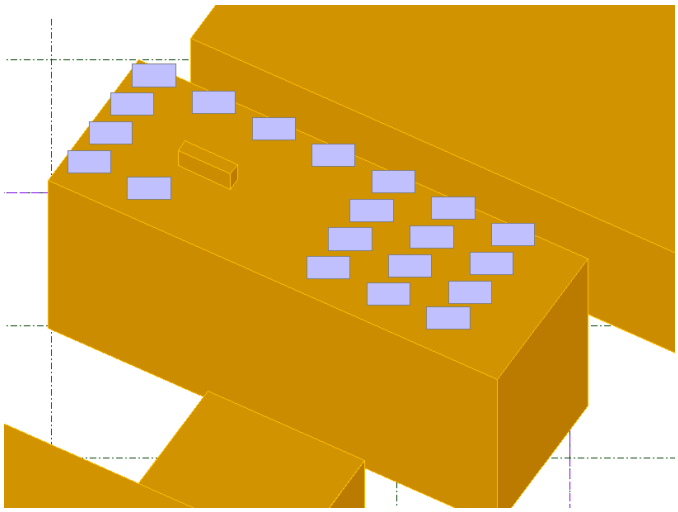

Figure 3.3 : Rooftop PV Installation in PV SYST

3.4 Comparison of Results

The monthly electrical energy predicted using ECOTECT and HOMER is higher than PV SYST. PV SYST considers the temperature effects and inverter efficiency to calculate the output electrical energy. ECOTECT neglects the temperature effects and HOMER does not consider surrounding shading effects. HOMER is suitable to use for PV in rural areas where the shading obstacles are easily avoidable. ECOTECT is highly desirable when thermal effects designed for the building engineering. Monthly electrical energy production using Sharp PV panels in HOMER, ECOTECT and PV SYST is compared in Figures 3.4, 3.5 & 3.6.

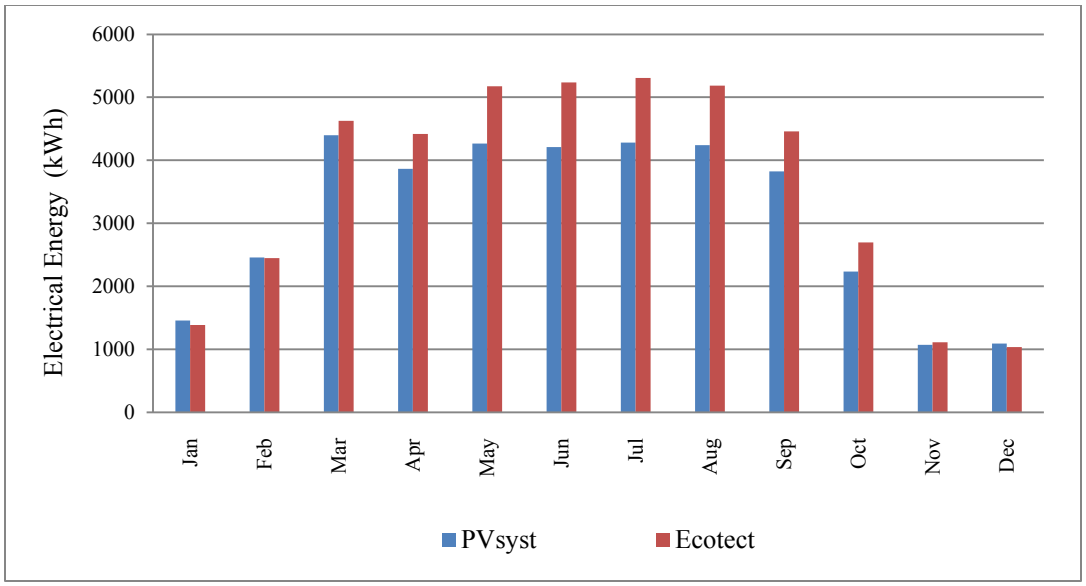

Figure 3.4 : Comparison of Monthly Electrical Energy Production with Sharp PV panels

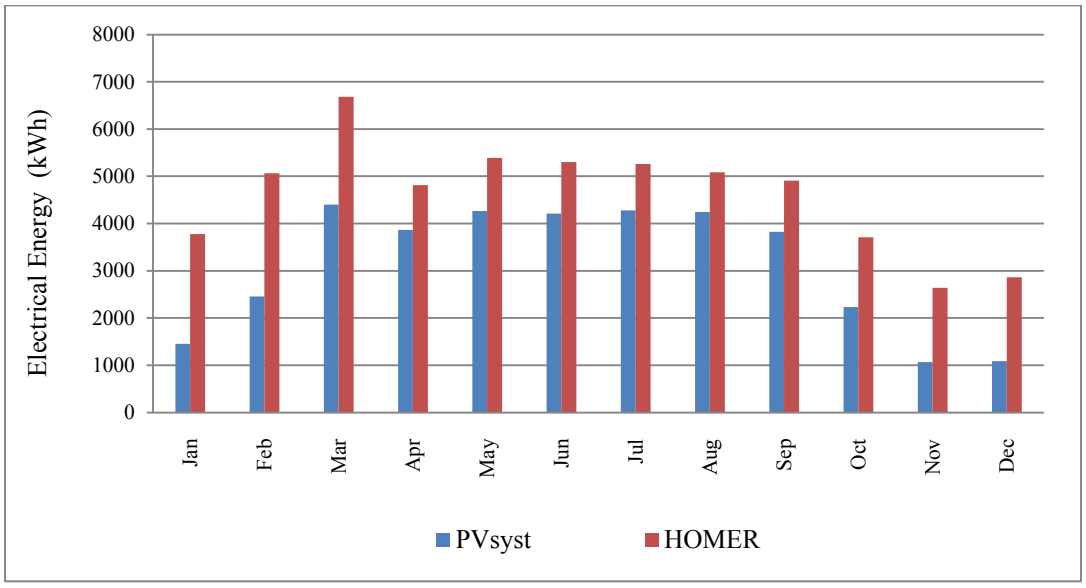

Figure 3.5 : Comparison of Monthly Electrical Energy Production with Sharp PV panels

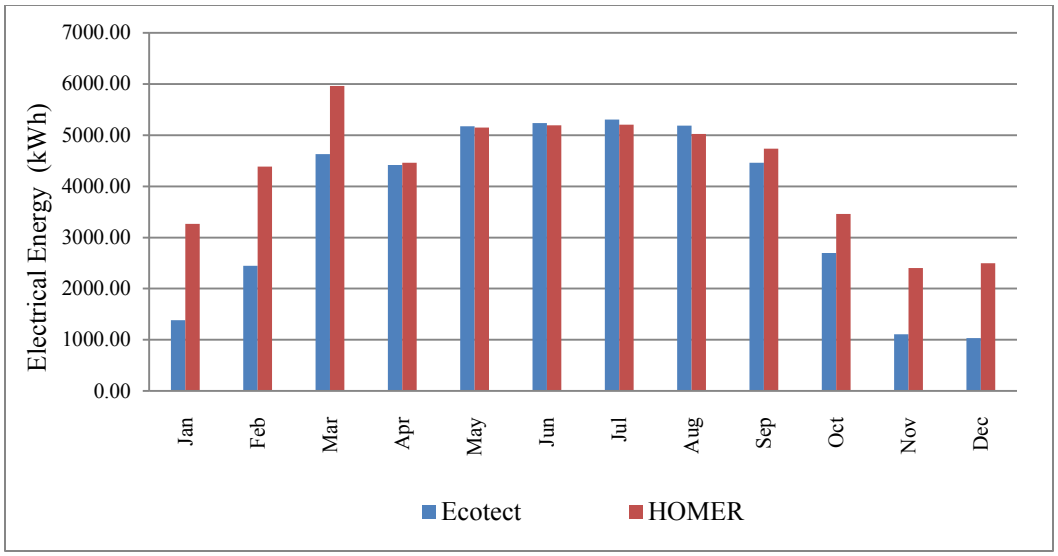

Figure 3.6 : Comparison of Monthly Electrical Energy Production with Sharp PV panels

A second case study was made with Canadian Solar PV panels which have a different output than Sharp PV panels. These PV panels are used for electrical energy production as well as building materials. A comparison for electrical energy production is represented in Figures 3.7, 3.8 & 3.9.

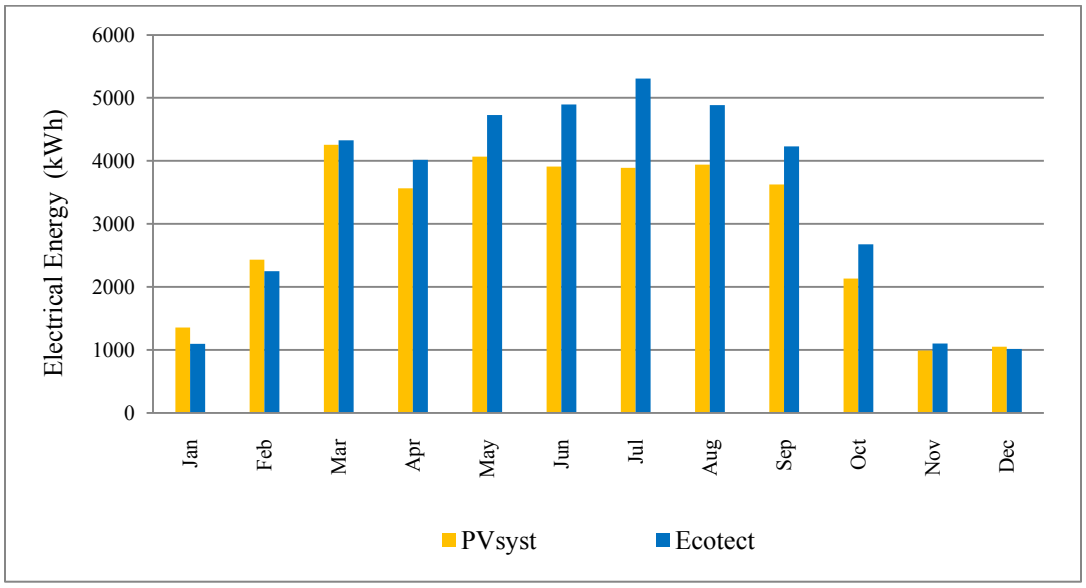

Figure 3.7 : Comparison of Monthly Electrical Energy Production with Canadian Solar PV panels

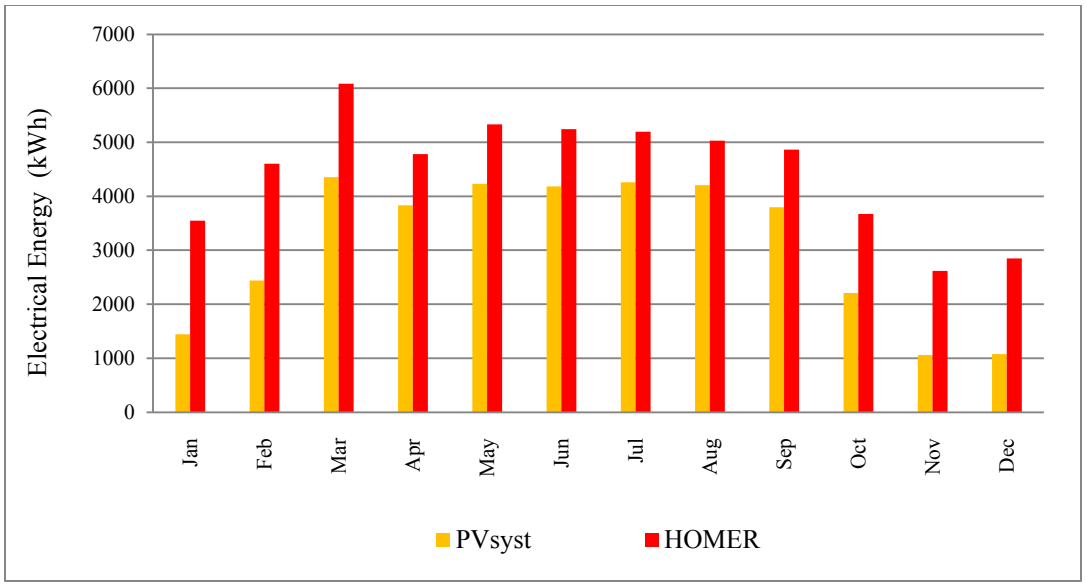

Figure 3.8 : Comparison of Monthly Electrical Energy Production with Canadian Solar PV panels

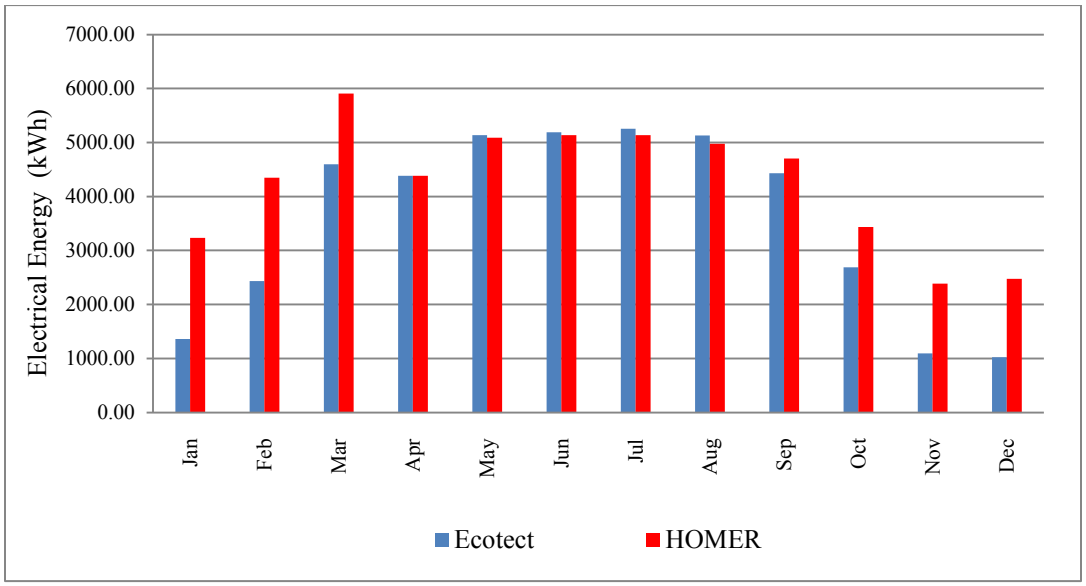

Figure 3.9 : Comparison of Monthly Electrical Energy Production with Canadian Solar PV panels

3.5 Conclusions

HOMER is mainly used for PV panel application in rural areas. It can be used to simulate different energy systems (wind energy, solar energy, fossil fuels) to obtain a realistic estimate of their capital and operating expenses. ECOTECT is more suitable when the thermal system is considered for design system with shading effects. PV SYST is an accurate tool to estimate the electrical energy production with PV panels in urban areas considering insolation, panel orientation, inverter efficiency, shading effects etc.

Chapter 4 : Increased Output as a Result of Prevailing Wind

Prevailing winds blow predominantly in a specific direction over the earth's surface. An areas' prevailing wind is generally affected by global atmospheric movement. The earth is encircled by several wide wind belts. These wind belts are determined by solar radiation and rotation of the earth. Hadley cell, Ferrel cell and Polar cell are the three main primary circulation cells. Prevailing winds forms due to unequal heating of earth. Hot air moves up and cooler air substitute's hot air and winds starts blowing. This difference in heating cause to flow air from equator to poles in the upper part of atmosphere and vice versa in the lower part of atmosphere. Prevailing winds blows quite frequently over the certain regions. Main prevailing winds are trade winds, westerlies, polar easterlies, jet streams etc. [43]. In rural areas, the standalone PV module tilt angle is set by considering the latitude of the location. In this chapter the cooling effect of the panel from the prevailing winds is analyzed. A model has been designed to calculate module temperature, output power and efficiency for various prevailing wind speeds. A detailed study of heat transfer through conduction, convection and radiation from the panel is also considered in the model.

4.1 Review of Previous Works

Duffie and Beckman have discussed solar irradiance, heat transer (conduction, convection & radiation), flat plat collector perormance etc. in different chapters of their book [44]. Nellis and Klein also discussed natural and forced convection co-relations for inclined surface in their book [45]. McAdams reports that the convection heat co-efficient can be calculated with wind speed from the following dimensionless equation [46].

$$h' = 5.7 + 3.8V \quad (4.1)$$

Where

h'=convection heat co-efficient (W/m^{2}K)

V=wind speed (m/s)

As above equation includes free convection and radiation, Watmuff et al. redefined the following equation [47].

$$h' = 2.8 + 3.0V \quad (4.2)$$

Sandia National Laboratory has designed a thermal model (SAND2004-3535) for back surface solar panel module temperature as follows [48].

$$T_m = E.\{e^{a+b.WS}\} + T_a \quad (4.3)$$

$$T_C = T_m + \frac{E}{E_0}.\Delta T \quad (4.4)$$

Where

T_a	Ambient temperature, ^{0}K
T_c	Cell temperature, ^{0}K
T_m	Module back temperature, ^{0}K
ΔT	Temperature difference between cell and module back, ^{0}K
E	Solar irradiance, W/m^2
E_0	Reference solar irradiance, normally 1000 W/m^2
WS	Wind speed at standard 10-m height, m/s
a & b	Empirical coefficients

In their thermal model a linear regression fit to the data provides the empirical values of coefficients (a and b). These values are mainly dependent on test equipments and site weather condition. King et al also analysed the temperature coeffficients for PV module

and array [49].

Oh et al. [50] worked with various components of silicon solar modules in the hot environment of Arizona as per IEC 61730-2 (international) and ANSI/UL 1703 (United States). They recommended short term and long term stress test for average temperature of various parts of the module, like short term and long term stress test for back sheet at 155^0C & 85^0C respectively.

Tang et al. [51] published their paper and derived module temperature as function of ambient temperature, wind speed, wind direction, total irradiance, and relative humidity; they also derived an equation with ambient temperature, wind speed and total irradiation as follows.

$$T_{module} = W1 * T_{ambient} + W2 * Irradiance + W3 * WindSpd + W4 * WindDir + W5 * Humidity + const \quad (4.5)$$

$$T_{module}(^0C) = 0.943 * T_{ambient} + 0.028 * Irradiance - 1.528 * WindSpd + 4.3 \quad (4.6)$$

Where

W1 Coefficient for temperature

W2 Coefficient for irradiance, ^{0}C/W.m^{-2}

W3 Coefficient for wind speed, ^{0}C/m.s^{-1}

W4 Coefficient for wind direction, ^{0}C/deg

W5 Coefficient for humidity, ^{0}C/RH%

The nominal operating cell temperature model (NOCT) for an open rack system is given

in equation 4.7 [52].

$$T_{module} = T_{ambient} + (T_{NOCT} - 20)x\left(\frac{Irradiance}{800}\right) \quad (4.7)$$

IEC 61853 standard has a thermal model for specific wind speed as follows [53].

$$T_{module} - T_{ambient} = bXG + a \quad (4.8)$$

4.2 Flat Plat Collector

In PV panels, a part of solar radiant energy is converted into electricity. The panel also acts like a heat exchanger to transform energy into heat loss through conduction, convection and radiation. As the incident radiant has a wavelength range mainly between 0.3 to 0.8 μm, so radiation loss become important for the panel. A considerable amount of work has been done in the thermodynamics and heat transfer regarding the solar collector. The model was developed based on flat plate solar collector characteristics. Equation 4.9 describes the balance of heat in a flat plate collector [44].

$$\eta = \frac{mc_p(T_p - T_a)}{A_c G_T} = \frac{Q_u}{A_c G_T} = F_g(\tau\alpha) - \frac{F_g U_L(T_p - T_a)}{G_T} \quad (4.9)$$

4.3 Heat Transfer Co-efficient

A two cover thermal network was considered for the thermal model. A detailed thermal network is shown in the figure 4.1, where T_p is the temperature of the plate and S is the solar energy available on the collector. This solar energy S is distributed into top losses, bottom losses, edge losses and energy gained in the collector.

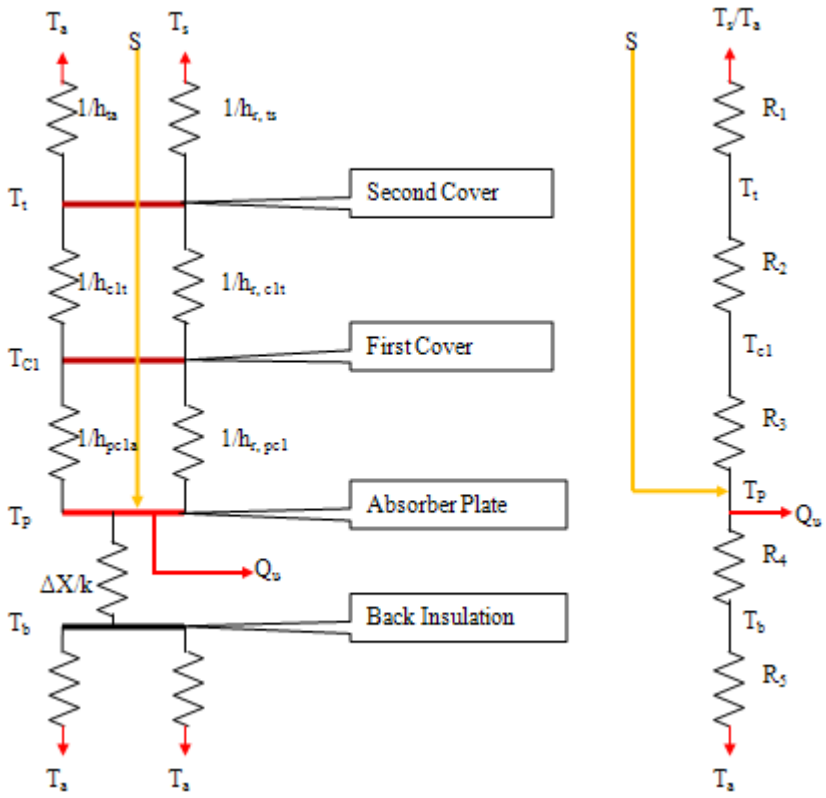

Figure 4.1 : Equivalent Thermal Network for Two Cover Flat Plate Collector

Top loss, bottom loss and edge loss co-efficient achieved through following equations.

$$U_t = \frac{1}{R_1 + R_2 + R_3} \tag{4.10}$$

$$U_b = \frac{1}{R_4 + R_5} \tag{4.11}$$

$$U_e = \frac{(UA)_{edge}}{A_c} \tag{4.12}$$

Where,

$$R_1 = \frac{1}{(5.7 + 3.8V) + \frac{(T_t + T_s)(T_t^2 + T_s^2)}{\frac{1}{\varepsilon_t} + \frac{1}{\varepsilon_s} - 1}} \tag{4.13}$$

$$R_2 = \frac{1}{\left(Nu\frac{k}{L_1}\right) + \frac{(T_t+T_{c1})(T_t^2+T_{c1}^2)}{\frac{1}{\varepsilon_t}+\frac{1}{\varepsilon_{c1}}-1}} \tag{4.14}$$

$$R_3 = \frac{1}{\left(Nu\frac{k}{L_2}\right) + \frac{(T_p+T_{c1})(T_p^2+T_{c1}^2)}{\frac{1}{\varepsilon_p}+\frac{1}{\varepsilon_{c1}}-1}} \tag{4.15}$$

$$R_4 = \frac{\Delta X}{k} \tag{4.16}$$

$$R_5 = \frac{1}{(5.7 + 3.8V) + \frac{(T_b+T_a)(T_b^2+T_a^2)}{\frac{1}{\varepsilon_b}+\frac{1}{\varepsilon_a}-1}} \tag{4.17}$$

In the MATLAB program above thermal equivalent network concept applied and results are summarized in table 4.1

4.4 Designing the Model

In the PV panel model, energy gained in the form of electricity with an efficiency provided by manufacturer at STC. Normally the bottom is well insulated with plywood or other materials, and the conduction loss through the bottom can be ignored. There is not a significant gap between the panel and glass cover.

Prevailing wind blows with velocity V and an angle m with the panel. A detailed schematic diagram is provided in figure 4.2.

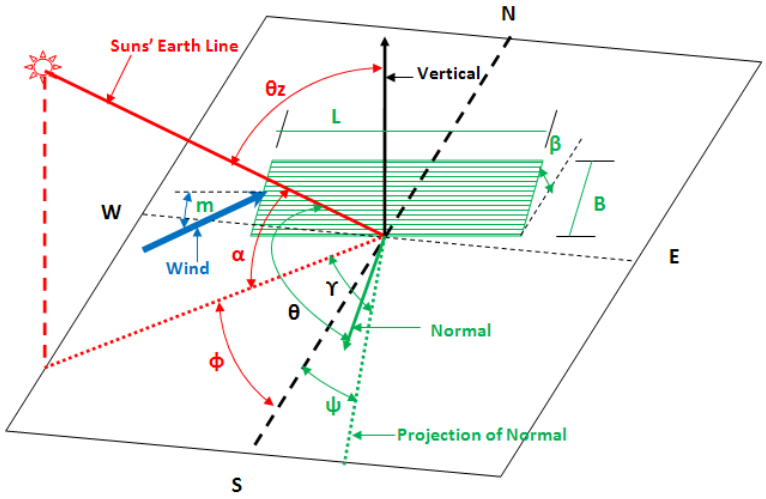

Figure 4.2 : Schematic Diagram for Prevailing Wind on PV Panel

For Natural Convection

Rayleigh Number with wind velocity component perpendicular the flow length [45],

$$R_a = \frac{g \sin\beta B^3 \beta'(\Delta T)}{(V \cos m)\alpha} \tag{4.18}$$

Where, B=Breadth of the Solar Module, α=Thermal Diffusivity, ΔT=Module Temp-Air Temp, V=Velocity of Prevailing Wind, β'=Volumetric Expansion Coefficient of Air and g =Gravitational Force

Then Nusselt Number for Natural Convection in inclined surface [15],

$$Nu_{nc} = 1 + 1.44\left[1 - \frac{1708(\sin 1.8\beta)^{1.6}}{Ra\cos\beta}\right]\left[1 - \frac{1708}{Ra\cos\beta}\right]^{+} + \left[\left(\frac{Ra\cos\beta}{5830}\right)^{1/3} - 1\right]^{+} \tag{4.19}$$

Then Natural Convection Co-efficient,

$$h_{nc} = \frac{Nu_{nc}k}{B} \tag{4.20}$$

$$h_{nc} = \frac{k}{B}\left(1 + 1.44\left[1 - \frac{1708(\sin 1.8\beta)^{1.6}}{Ra\cos\beta}\right]\left[1 - \frac{1708}{Ra\cos\beta}\right]^{+} + \left[\left(\frac{Ra\cos\beta}{5830}\right)^{1/3} - 1\right]^{+}\right) \tag{4.21}$$

$$h_{nc} = \frac{k}{B}\left(1 + 1.44\left[1 - \frac{1708(V\cos m)\alpha(\sin 1.8\beta)^{1.6}}{g\sin\beta B^3\beta'(\Delta T)\cos\beta}\right]\left[1 - \frac{1708(V\cos m)\alpha}{g\sin\beta B^3\beta'(\Delta T)\cos\beta}\right]^{+} + \left[\left(\frac{g\sin\beta B^3\beta'(\Delta T)}{(V\cos m)\alpha}\frac{\cos\beta}{5830}\right)^{1/3} - 1\right]^{+}\right) \tag{4.22}$$

For Forced Convection

Reynold Number with wind velocity component along the flow length [45],

$$Re = \frac{\rho LV\cos a}{\mu} \tag{4.23}$$

Where, ρ=Density of Air, μ=Viscosity of Air and L=Length of the Module

Then Nusselt Number for Forced Convection [44],

$$Nu_{fc} = 0.86Re^{1/2}Pr^{1/3} \tag{4.24}$$

$$Nu_{fc} = 0.86\left(\frac{\rho LV\cos m}{\mu}\right)^{1/2}Pr^{1/3} \tag{4.25}$$

Then Forced Convection Co-efficient,

$$h_{fc} = \frac{Nu_{fc}k}{L} \tag{4.26}$$

$$h_{fc} = \frac{k}{L}\left(0.86\left(\frac{\rho LV\cos m}{\mu}\right)^{1/2} Pr^{1/3}\right) \tag{4.27}$$

Where,

Ra	Rayleigh number
g	Gravitational force, m/s^2
β	Tilt angle, degree
β’	Volumetric co-efficient
m	Wind angle with module, deg
Nu	Nusselt number
h	Heat transfer co-efficient, W/m^2K

For Natural and Forced Convection

Thus Total Convection for Natural and Forced Convection [45],

$$h_{tc} = \left[\left\{\frac{k}{B}\left(1 + 1.44\left[1 - \frac{1708(V\cos m)\alpha(\sin 1.8\beta)^{1.6}}{g\sin\beta B^3\beta'(\Delta T)\cos\beta}\right]\left[1 - \frac{1708(V\cos m)\alpha}{g\sin\beta B^3\beta'(\Delta T)\cos\beta}\right]^{+} + \left[\left(\frac{g\sin\beta B^3\beta'(\Delta T)}{(V\cos m)\alpha}\frac{\cos\beta}{5830}\right)^{1/3} - 1\right]^{+}\right)\right\}^3 + \left\{\frac{k}{L}\left(0.86\left(\frac{\rho LV\cos m}{\mu}\right)^{1/2} Pr^{1/3}\right)\right\}^3\right]^{1/3} \tag{4.28}$$

Equations 4.1 and 4.2 were redefined with prevailing wind angle in equations 4.29 and 4.30 respectively and compared with equation 4.28.

$$h' = 5.7 + 3.8Vcos(m) \quad (4.29)$$

$$h' = 2.8 + 3.0Vcos(m) \quad (4.30)$$

The main objective of the model is to establish the effect of wind speed and direction on efficiency. Applying the thermal model (figure 4.3) the panel temperature is calculated through a MATLAB iteration process for various wind speeds and directions. Electrical output was also available from heat balance equations as per table 4.1& 4.2. It has been observed that natural convection loss from the top and the bottom of the inclined surface was negligible compared to forced convection loss.

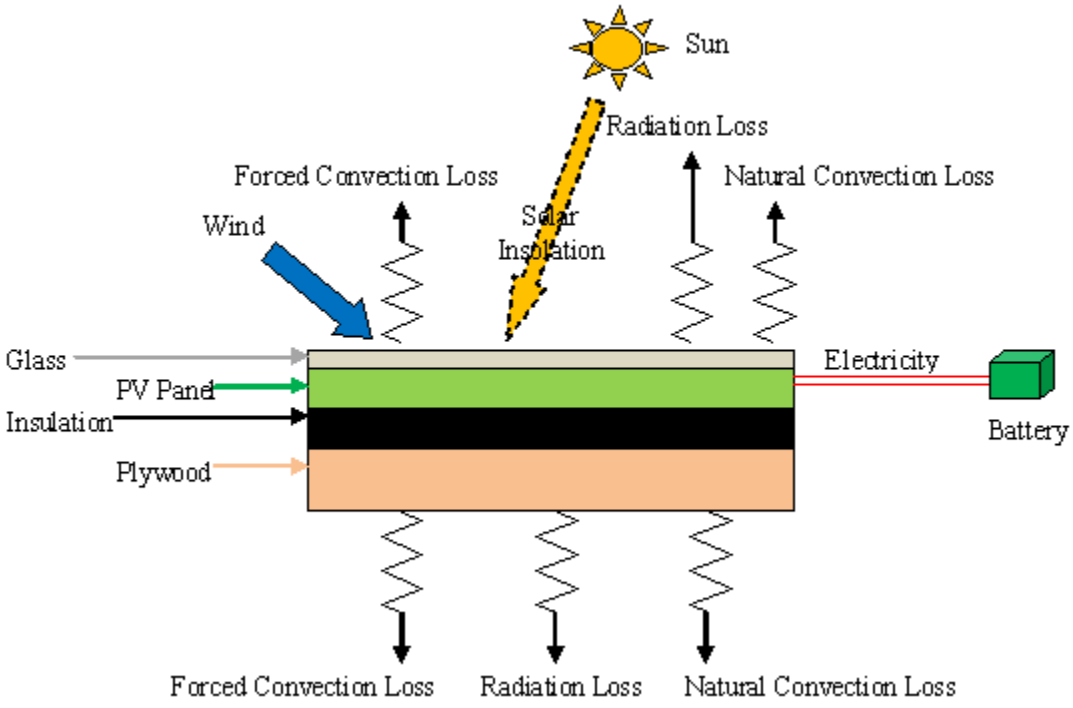

Figure 4.3 : Thermal Model of Standalone PV Module

Table 4.1 : Effect of Output Power in Various Wind Speed

Wind Velocity (m/s)		**0.0**	**1.0**	**2.0**	**3.0**	**4.0**	**5.0**
T_p	^0C	**69.15**	**57.46**	**50.5**	**45.95**	**42.75**	**40.39**
T_p	^0K	**342.15**	**330.46**	**323.5**	**318.95**	**315.75**	**313.39**
$r_{convectiontop}$	m^2K/W	0.1754	0.1053	0.0752	0.0585	0.0478	0.0405
$q_{convectiontop}$	W/m^2	251.7	308.4	339.2	358.2	371.0	380.1
$r_{radiationtop}$	m^2K/W	0.2291	0.2428	0.2515	0.2573	0.2615	0.2646
$r_{radiationback}$	m^2K/W	0.2230	0.2362	0.2445	0.2501	0.2541	0.2571
$q_{radiationtop}$	W/m^2	218.9	158.4	125.3	104.7	90.8	80.8
q_{front} (from PV to Air & Sky)	W/m^2	471	467	464	463	462	461
q_{back}	W/m^2	450	446	443	442	441	440
Electrical Power (W/m^2)		79	88	92	95	98	99
q_{total}	W/m^2	1000	1000	1000	1000	1000	1000
Efficiency		7.9%	8.8%	9.2%	9.5%	9.8%	9.9%
Variance in Efficiency			10.1%	16.2%	20.1%	22.9%	25.0%

Table 4.2 : Effect of Various Wind Directions on Output Power

Wind Angle of Attack (deg)		0	15	30	45	60	75
T_p	^0C	**40.38**	**40.75**	**41.88**	**44.1**	**48**	**55.06**
T_p	^0K	**313.38**	**313.75**	**314.88**	**317.1**	**321**	**328.06**

Wind Angle of Attack (deg)		0	15	30	45	60	75
$r_{convectiontop}$	m^2K/W	0.0405	0.0416	0.0451	0.0523	0.0658	0.0942
$q_{convectiontop}$	W/m^2	379.9	378.8	374.0	365.5	349.6	319.2
$r_{radiationtop}$	m^2K/W	0.2646	0.2642	0.2626	0.2597	0.2546	0.2458
$r_{radiationback}$	m^2K/W	0.2571	0.2566	0.2552	0.2524	0.2475	0.2390
$q_{radiationtop}$	W/m^2	80.8	82.3	87.1	96.6	113.9	146.7
q_{front} (from PV to Air & Sky)	W/m^2	461	461	461	462	463	466
q_{back}	W/m^2	440	440	440	441	443	445
Electrical Power (W/m^2)		99	99	98	97	94	89
q_{total}	W/m^2	1000	1000	1000	1000	1000	1000
Efficiency		9.9%	9.9%	9.8%	9.7%	9.4%	8.9%
Variance in Efficiency			-0.3%	-1.0%	-2.6%	-5.3%	-10.3%

The panel temperature decreases with increase in wind speed. Approximately 28.8°C temperature decrease with 5 m/s wind velocity increase over the panel. Also wind direction variation from 0 to 75 degrees cooled the panel almost 14.7°C. These results are represented graphically in figures 4.4 and 4.5.

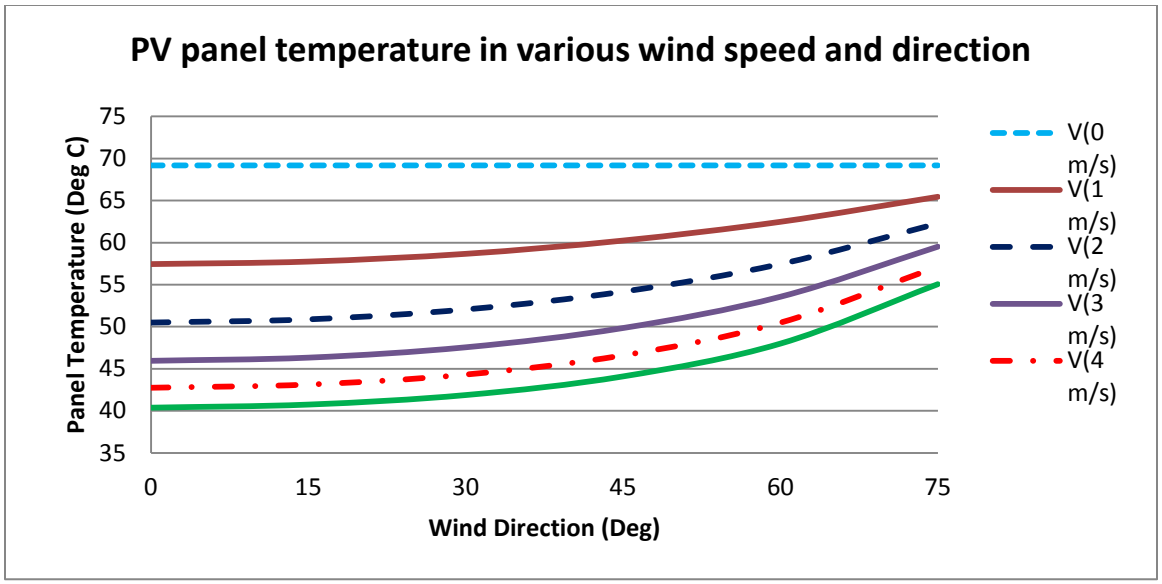

Figure 4.4 : Changes of Temperature in Various Wind Speed and Direction (Calculated)

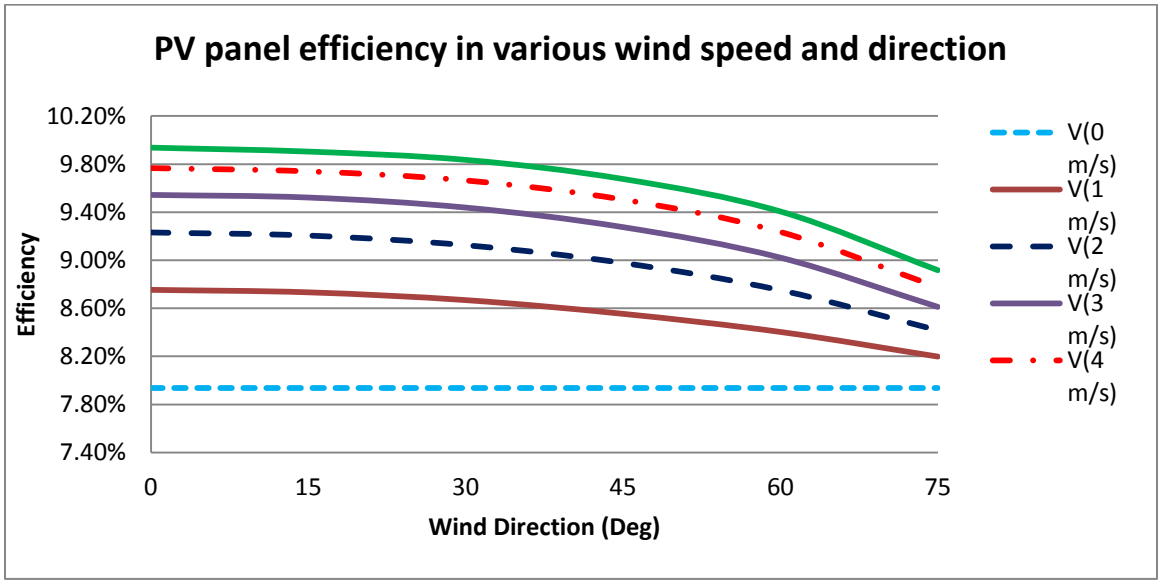

Figure 4.5: Changes of Efficiency in Various Wind Speed and Direction (Calculated)

4.5 Experimental Setup and Results

Experiment Setup

The Department of Building, Civil & Environmental Engineering has installed a state of the art solar simulator laboratory in the Hall building which is still not fully commissioned. Some test were done in this lab with manual calibration.

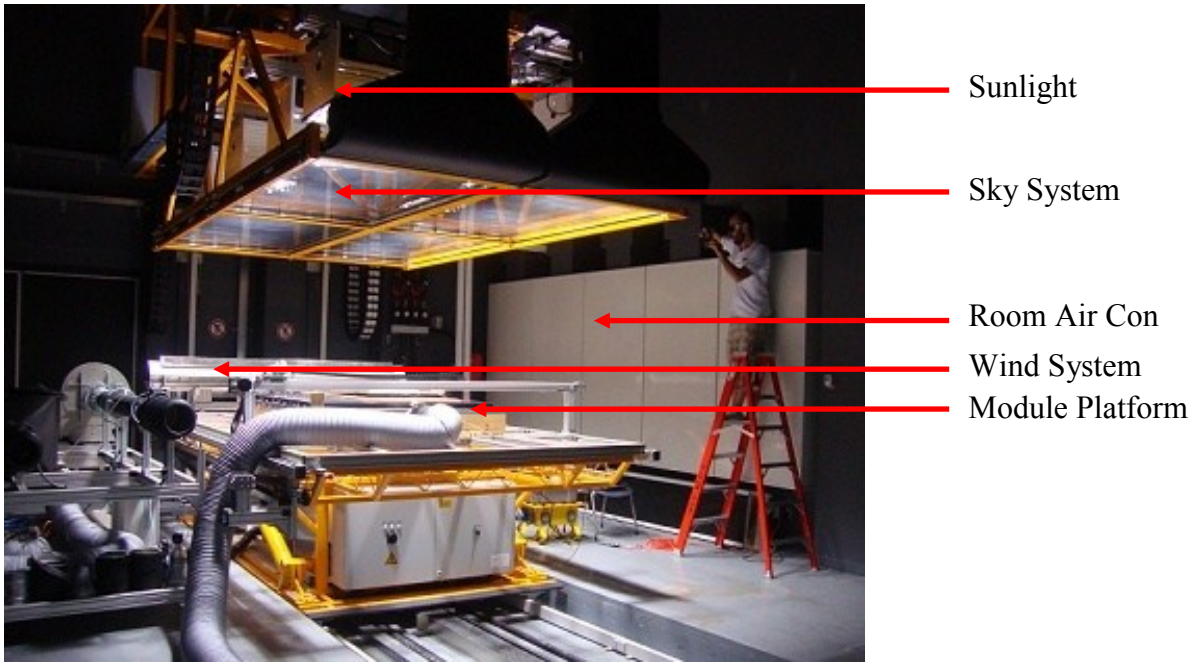

Figure 4.6 : Setup for the experiment in solar simulator lab

More than two hours was required to calibrate the whole setup. In future, after the final commissioning the system will not require any manual calibration.

Figure 4.7 : Calibration in-process for the whole setup

All instruction for movement of the sun system and solar panel base along with wind system was done through the interactive console.

a. Instruction in the console

b. Results in the setup

Figure 4.8 : Instruction from the console and correspondent equipment position

Figure 4.9 : Adjustment of solar irradiation over the module

To ensure uniform irradiance over the panel surface, instruction was given through the console to pyranometer and sun system to adjust for minimum variance. In figure 4.9, as per assigned area average value and variance of irradiance was recorded. The system also provided the average, minimum and maximum value for the overall area.

Two thermocouples were placed on the top and bottom of the solar panel to obtain temperatures. Labview software stored the temperature data at minute intervals. Variable resistors with 11 amps current ratings were connected to the solar panels to measure maximum power, current and voltage at maximum power. An I-V tracer was used to obtain the I-V curves for poly and mono crystalline PV modules. An Ameter and a

voltmeter were used to measure the output power of the panels at different conditions and also to verify the I-V tracer readings..

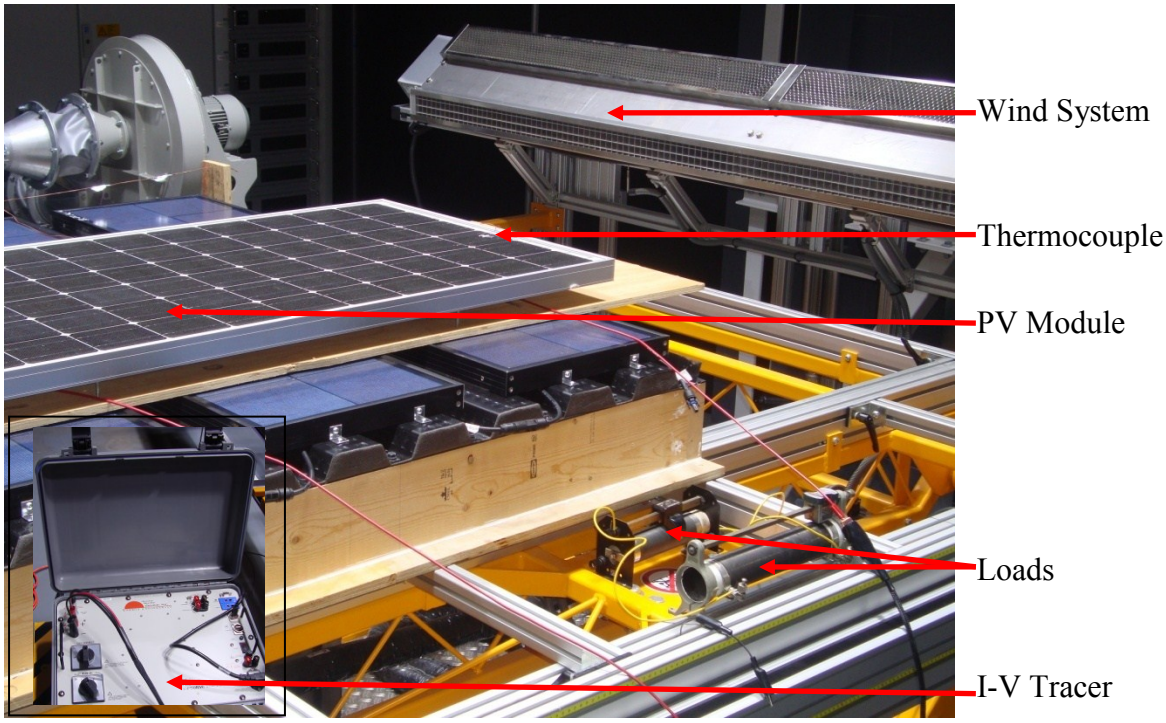

Figure 4.10 : Measurement of output power and I-V curve

Results

SIEMENS SM110 mono-crystalline solar module was used in the experiment. Resistance at maximum power was obtained from the technical specification sheet as 2.77 Ω ($110/6.3^2$). This resistance was setup in the two parallel resistances with 11 Amps rating. The following results were obtained in maximum wind and no wind conditions.

Maximum Wind Condition for Mono-crystalline

V_{oc} = 20.43 Volts

I_{sc} = 6.73 Amps

At 2.77 Ω, V_m = 15.86 Volts; I_m = 6.03 Amps; P_m = 95.6 Watts

No Wind Condition for Mono-crystalline

V_{oc} = 17.67 Volts

I_{sc} = 6.79 Amps

At 2.77 Ω, V_m = 13.21 Volts; I_m = 5.91 Amps; P_m = 78.10 Watts

Maximum Wind Condition for Poly-crystalline

V_{oc} = 10.36 Volts

I_{sc} = 6.76 Amps

At 1.2 Ω, V = 7.65 Volts; I_m = 6.3 Amps; P_m = 48.3 Watts

The maximum wind generation capability of the system is 4 m/s.

Top temperatures of the module are represented in table 4.7.

Table 4.3 : Top thermocouple temperature of the module

Time	Module Temp [°C]	
7:02 PM	43.6	With maximum wind & load connected
7:06 PM	50.5	
7:07 PM	52	
7:08 PM	53.4	
7:16 PM	63.2	
7:16 PM	63.9	
7:17 PM	64.8	
8:03 PM	72.5	
8:04 PM	72.5	Without wind & load connected

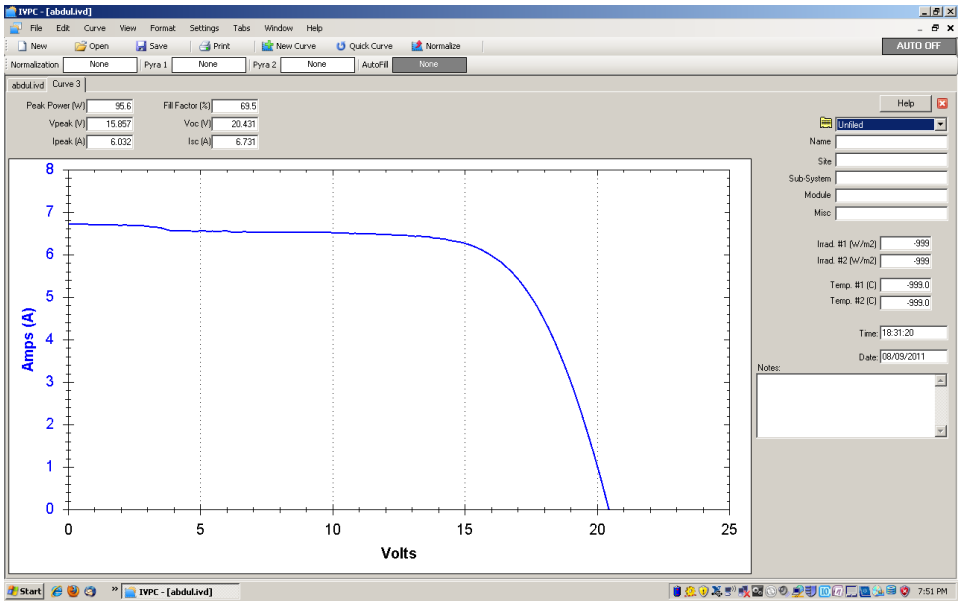

Figure 4.11 : I-V curve plotted by I-V tracer for mono-crystalline with wind

Output power also obtained through I-V tracer as per figures 4.12 and 4.13; values are 95.6 watts and 78.1 watts with and without wind respectively. Fill factor, open circuit voltage, and short circuit current, voltage at peak power and current at peak power also recorded for both conditions through I-V tracer software.

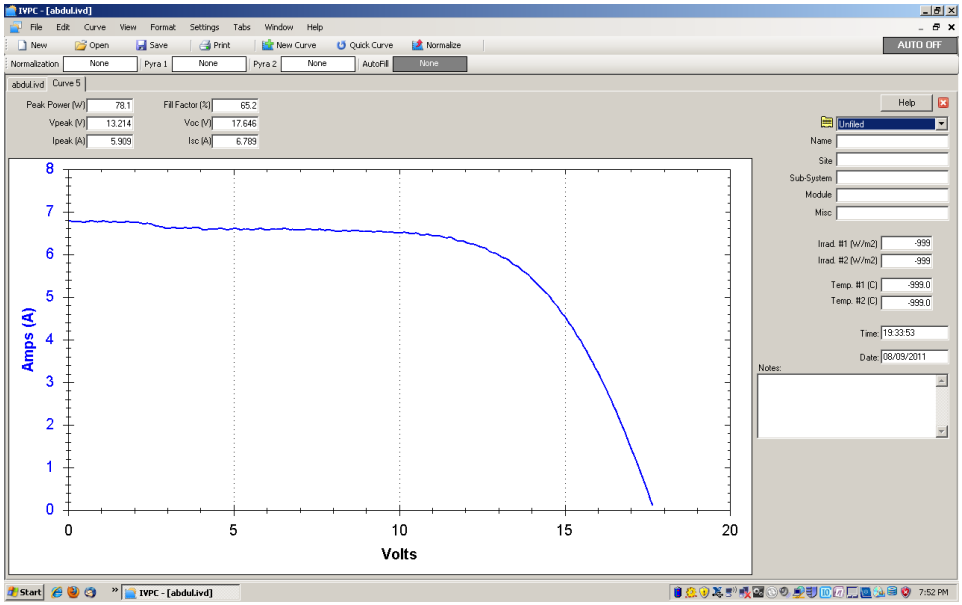

Figure 4.12 : I-V curve plotted by I-V tracer for mono-crystalline without wind

Comparison of Results

Table 4.4 : Variance between model and experiment results

	Model	**Experiment**	**Variance**
No wind condition Module top temperature	69.15^{o} C	72.5^{o} C	4.8%
Maximum wind condition (4 m/s) Module top temperature	42.75^{o} C	43.6^{o} C	2%
No wind condition Output power (watts) Efficiency (%)	79 watts 7.9%	78.1 watts 7.3%	1.1% 7.6%
Maximum wind condition (4 m/s) Output power (watts) Efficiency (%)	98 watts 9.8%	95.6 watts 8.98%	2.5% 8.4%
Improvement in output power and efficiency (from no wind to 4 m/s wind)	22.9%	22.4%	2.2%

In the model all temperatures were calculated based on 1000 W/m^2 irradiance. In the experiment setup average irradiance was 1065 W/m^2 with a minimum 984 W/m^2 and a maximum 1113 W/m^2. As a result, experiment temperatures were higher than the model temperatures. In experiment, output powers are lower due to line losses, which were not considered in the model.

4.6 Conclusions

There is a good agreement between the thermal model temperatures and experiment results. So from the thermal model and laboratory experiment it has been observed that prevailing wind reduced the module temperature. Finally the efficiency of the mono-crystalline panel was improved 22.4% due to variation of wind speed from zero to maximum wind speed (4 m/s) of the system.

Chapter 5 : Impact of Temperature Variation in a Module

Solar cells are susceptible to temperature like other semiconductor equipment. Variation in temperature changes the band gap energy in semiconductor materials which affects the semiconductor parameters. Increasing semiconductor temperature decreases band gap energy, and increases energy in the electrons of semiconductor. Thus increase in temperature reduces the band gap and band gap energy in the semiconductor band gap model.

Variation in temperature predominantly affects the open circuit voltage of solar cell, figure 5.1 shows small increment in short circuit current but higher decrease in open circuit voltage with increase in cell temperature.

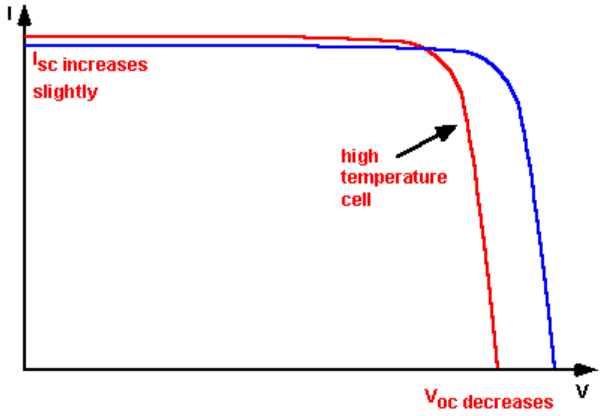

Figure 5.1 : Effect of Temperature in I-V Curve

5.1 Effect of Temperature on PV Cells and Modules

The dark saturation current (I_0) mainly causes the decrease in open circuit voltage with increase in temperature. Following equation provides I_0 in a p-n junction [54].

$$I_0 = qA\frac{Dn_i^2}{LN_D} \tag{5.1}$$

Few parameters in the above equation have temperature dependents, intrinsic carrier concentration (n_i) is the most significant among those. Higher temperature gives higher intrinsic carrier concentration and lower band gap energy. The intrinsic carrier concentration equation is provided below [54].

$$n_i^2 = 4\left(\frac{2\pi kT}{h^2}\right)^3 (m_e^* m_h^*)^{3/2} exp\left(-\frac{E_{G0}}{kT}\right) = BT^3 exp\left(-\frac{E_{G0}}{kT}\right) \tag{5.2}$$

Placing these values in intrinsic carrier concentration equation and ignoring temperature effect on other parameters, following equation is available.

$$I_0 = qA\frac{D}{LN_D}BT^3 exp\left(-\frac{E_{G0}}{kT}\right) \approx B'T^{\gamma} exp\left(-\frac{E_{G0}}{kT}\right) \tag{5.3}$$

Hence open circuit voltage (V_{oc}) is available as follows.

$$\begin{aligned} V_{OC} &= \frac{kT}{q} ln\left(\frac{I_{SC}}{I_0}\right) = \frac{kT}{q}[lnI_{SC} - lnI_0] \\ &= \frac{kT}{q} lnI_{SC} - \frac{kT}{q} ln\left[B'T^{\gamma} exp\left(-\frac{qV_{G0}}{kT}\right)\right] \\ &= \frac{kT}{q}\left(lnI_{SC} - lnB' - \gamma lnT + \frac{qV_{G0}}{kT}\right) \end{aligned} \tag{5.4}$$

Thus,

$$\frac{dV_{OC}}{dT} = -\frac{V_{G0} - V_{OC} + \gamma\frac{kT}{q}}{T} \approx -2.2mV\ per\ \deg C\ for\ Si \tag{5.5}$$

$$\frac{1}{I_{SC}}\frac{dI_{SC}}{dT} \approx 0.0006\, per\ \deg C\ for\ Si \tag{5.6}$$

Solar cells are connected in series and parallel depending on the requirement of voltage and current ratings respectively. In general PV module is built to charge 12 volts battery. Solar cell has a voltage of 0.6 V under STC (25^{o} C and AM 1.5 illumination). For higher charging voltage a panel is generally made of 36 cells (Figure 5.2) where open circuit voltage is 21 V. In STC for maximum power operating voltage become 17 or 18 V for such panel. This extra voltage helps to encounter voltage drop in PV systems and lower insolation.

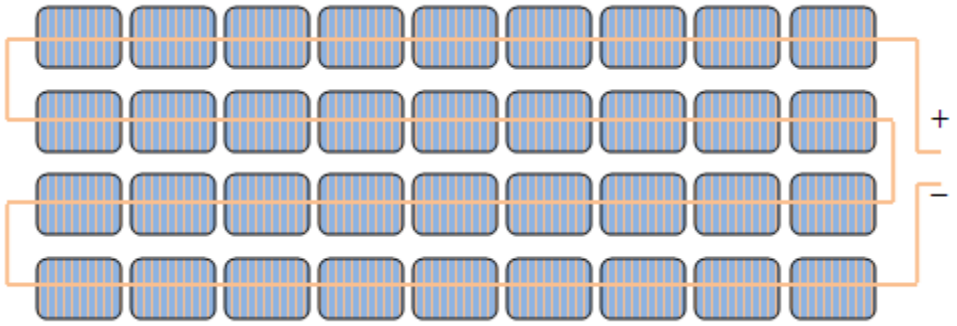

Figure 5.2 : A Typical PV Module with 36 Series Connected Solar Cells

5.2 Review of Previous Works

Temperature variation in cells within a module has been studied due to short circuit current and open circuit voltage by many researchers. Mismatch occurs due to temperature variation in PV modules and arrays.

Koirala et al. developed static and dynamic mismatches models and also analyzed various results for homogeneous and partial shading mismatch losses in modules and arrays [55]. Picault et al. carried out a mismatch case study in Jaen University campus (Spain) for

partial shading; they proposed an alternative connection scheme to combat 4.8% power loss due to mismatch [56]. Hiren Patel and Vivek Agarwal developed a MATLAB model to simulate the partial shading effect on large PV plant [57].

5.3 Model for Open Circuit Voltage Due to Temperature Variations

Assuming different temperatures in cells a study is made to observe the corresponding variation in open circuit voltage. In table 5.1, various cell temperatures available from figure 5.5 to obtain the module open circuit voltages. Module temperature varying from 54.6^{o}C to 61.8^{o}C provides a 18.87 volts open circuit voltage.

Table 5.1 : Variations in module open circuit voltage due to variation in cells temperature

Ambient temp (^{o}C)		**25**
V_{oc} at ambient temp and 1.5 AM (Volts)		**0.6**
Reduction in V_{oc} per ^{o}C for Si (Volts/^{o}C)		**0.00227**
Nos. of Cell in Series		**36**
	Temp (^{o} C)	**V_{oc}(Volts)**
Cell1	59.4	0.522
Cell2	59.4	0.522
Cell3	59.3	0.522
Cell4	59.3	0.522
Cell5	54.6	0.533
Cell6	54.6	0.533
Cell7	61.1	0.518
Cell8	61.1	0.518
Cell9	60.8	0.519
Cell10	60.8	0.519
Cell11	57.6	0.526
Cell12	57.6	0.526
Cell13	61.2	0.518
Cell14	61.2	0.518
Cell15	61.8	0.516
Cell16	61.8	0.516
Cell17	57.8	0.525
Cell18	57.8	0.525
Cell19	60.2	0.520

Cell20	60.2	0.520
Cell21	60.4	0.520
Cell22	60.4	0.520
Cell23	56.2	0.529
Cell24	56.2	0.529
Cell25	59.5	0.522
Cell26	59.5	0.522
Cell27	58.7	0.523
Cell28	58.7	0.523
Cell29	55.2	0.531
Cell30	55.2	0.531
Cell31	57.2	0.527
Cell32	57.2	0.527
Cell33	56	0.530
Cell34	56	0.530
Cell35	54.6	0.533
Cell36	54.6	0.533

Model Module Voc	**18.87**	**Volts**

5.4 Experimental Setup and Results

Experimental Setup

For poly-crystalline module, 30 thermocouples were connected and for mono-crystalline 2 thermocouples were connected for temperature records. But in both cases, temperature was recorded by FLIR 800 infra red camera. Infra red images were analyzed by the software for temperature variations. All other setups remained unchanged compared to thermal model experiment.

Results

In poly-crystalline module we have observed 10.9^{o}C temperature variation within the 18 cells. In figure 5.3, infra red images clearly indicate the temperature variations in the module. A FLIR 800 infra red camera was used to take the pictures. After taking the

picture temperature variations were indicated by the software provided for FLIR 800 camera.

Figure 5.3 : Temperature variation in poly-crystalline module surface

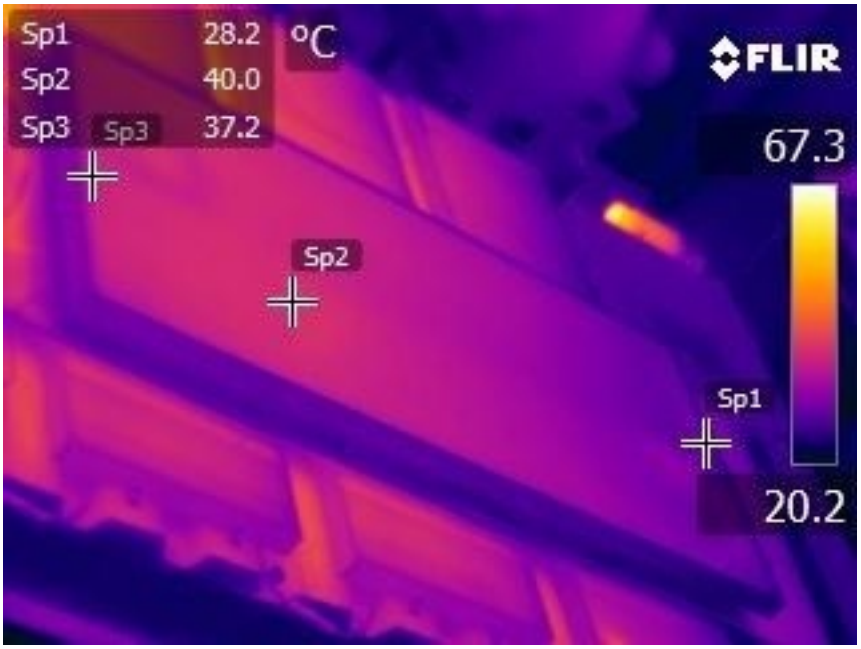

Figure 5.4 : Temperature variation in mono-crystalline module with wind

In figure 5.4 mono-crystalline module cells temperature variation with wind is clearly

visible with various hot spots. Near the wind system panel was cooler (28.2^{o}C) than the further edge (37.2^{o}C). But the highest hot spot was identified in Sp2 (40.0^{o}C).

Mono-crystalline module without wind had a very high temperature (more than 70^{o}C) in the cells; figure 5.5 clearly defines the distribution. Temperature was measured in total 18 spots with highest and lowest temperatures 61.8^{o}C and 54.6^{o}C respectively in no wind condition.

Open circuit voltage was calculated considering temperature distribution in figure 5.5 as follows. In the same time it was compared with measured open circuit voltage in no wind condition. All measurements were done on the surface glass cover of the module.

V_{oc} at STC from SIEMENS 110 specification = 21.7 Volts

V_{oc} calculated in model, with various temperature distribution = 18.87 Volts

V_{oc} measured in experiment, in no wind condition = 17.65 Volts

Variation in V_{oc} between model and experiment = 6.5%

Measurements	°C
Sp1	59.4
Sp2	59.3
Sp3	54.6
Sp4	61.1
Sp5	60.8
Sp6	57.6
Sp7	61.2
Sp8	61.8
Sp9	57.8
Sp10	60.2
Sp11	60.4
Sp12	56.2
Sp13	59.5
Sp14	58.7
Sp15	55.2
Sp16	57.2
Sp17	56.0
Sp18	54.6

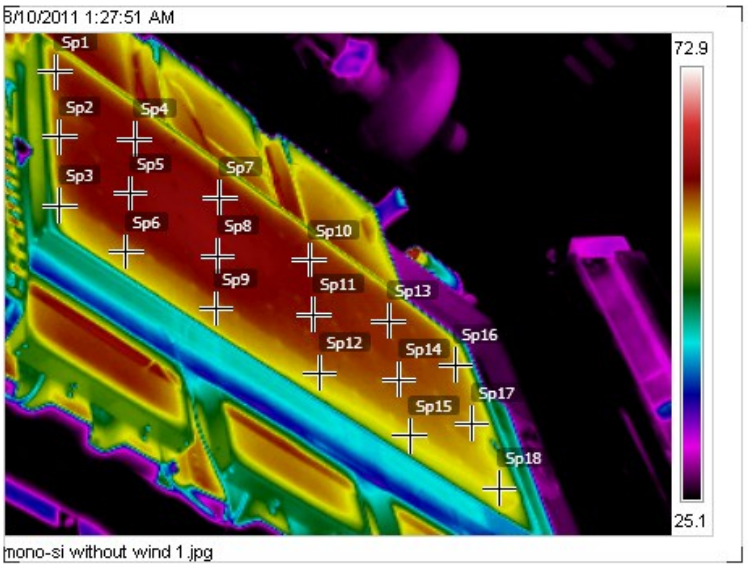

Figure 5.5 : Temperature variation in mono-crystalline module without wind

It has been observed that infra red camera provides temperature lower than temperature measured by thermocouple. 36 thermocouples for 36 cells would provide more accurate results than the infra red camera output.

5.5 Conclusions

Temperature variation in solar cells either due to design errors or manufacturing defects has been observed in the experiment. In our experiment a variation of 10.9^{o}C was available for poly-crystalline module. In mono-crystalline module 11.8^{o}C temperature variations observed with wind. Such temperature difference was only 7.2^{o}C in case of no wind condition. The variation in open circuit voltage between STC and model was 13%, whereas STC and the measured was 19%. This conforms that the cell temperatures are higher than cover glass temperatures. Variation between measured and model open circuit voltage was 6.5%.

Chapter 6 : Future Work

Solar simulator laboratory equipment has not been commissioned yet with 100% accuracy. The manufacturer is working remotely to commission the system from Germany. Hopefully the whole system will be commissioned soon with proper calibration of sun system, wind system, panel base, hot air system etc.

After the commissioning it will be very convenient to run the experiment without any delay due to balancing and calibration. The wind measurement will be perfect for the system. Incident irradiance distribution will be directly performed by the console itself.

In existing system wind always blows parallel to the solar module. An additional wind system could be installed to make an angle between the wind and solar module. Thus the model for wind direction can be easily verified in this laboratory.

Changes of ambient temperature will also allow performing experiment for STC and NOTC conditions. Various sky conditions will also explain the behavior of solar modules accordingly. More thermocouple connections (at least 72) will increase reliability and accuracy of the experiment.

References

[1]. U.S. Department of Energy,"International Energy Outlook 2010" [Online] July 27, 2010. [Cited: July 24, 2011.] http://www.eia.gov/oiaf/ieo/world.html.

[2]. Smil, V., General Energetics: Energy in the Biosphere and Civilization. General Energetics: Energy in the Biosphere and Civilization. Winnipeg : John Wiley & Sons, 1991, p. 240.

[3]. Smil, V., Energy: A Beginner's Guide. Winnipeg : Oneworld, 2006. p. 12.

[4]. Archer, Cristina L and Jacobson, Mark J., Evaluation of global wind power. 2005, Journal of Geophysical Research - Atmospheres, p. 46.

[5]. FAO, UN, "Energy conversion by photosynthetic organisms" Renewable biological systems for alternative sustainable energy production. [Online] 2008. [Cited: July 24, 2011.] http://www.fao.org/docrep/w7241e/w7241e06.htm#TopOfPage.

[6]. U.S. EIA, Energy, "International Energy Annual 2006", U.S. Energy Information Administration. [Online] June-December 2008. [Cited: July 24, 2011.] http://www.eia.gov/emeu/iea/Notes%20for%20Table%201_8.html.

[7]. U.S. EIA, Electricity, "International Energy Annual 2006", Independent Statistics and Analysis. [Online] June-December 2008. [Cited: July 24, 2011.] http://www.eia.gov/iea/elec.html.

[8]. Naylor, Mark F. and Farmer, Kevin C., "Sun Damage and Prevention", The Electronic Textbook of Dermatology. [Online] 1995. [Cited: July 24, 2011.] http://www.telemedicine.org/sundam/sundam2.4.1.html.

[9]. Honsberg, Christiana and Bowden, Stuart, "Photon Flux", PVEDUCATION, [Online] 2010. [Cited: July 24, 2011.] http://www.pveducation.org/pvcdrom/properties-of-sunlight/photon-flux.

[10]. Parrott, J. E., *Choice of an equivalent black body solar temperature.* 1993, Solar Energy, pp. 195-195.

[11]. Honsberg, Christiana and Bowden, Stuart., "The Sun", PVEDUCATION, [Online] 2010. [Cited: July 24, 2011.] http://www.pveducation.org/pvcdrom/properties-of-sunlight/the-sun#ref2.

[12]. Honsberg, Christiana and Bowden, Stuart., "The Sun", PVEDUCATION, [Online] 2010. [Cited: March 7, 2012.] http://www.pveducation.org/pvcdrom/properties-of-sunlight/the-sun.

[13]. Honsberg, Christiana and Bowden, Stuart, "Solar Radiation in Space", PVEDUCATION, [Online] 2010. [Cited: February 29, 2012.] http://www.pveducation.org/pvcdrom/properties-of-sunlight/solar-radiation-in-space.

[14]. Athienitis, A.K., *Building Thermal Analysis,* 2nd Edition. Boston : s.n., 1999.

[15]. Duffie, John A. and Beckman, William A., *Solar Engineering of Thermal Processe,* Wisconsin : John Wiley & Sons, 2006.

[16]. Jhon Twidell, Tony Weir, *Renewable Energy Resources,* New York : Taylor and Francis, 2006. ISBN.

[17]. Honsberg, Christiana and Bowden, Stuart, "Solar Cell Structure" PVEDUCATION, [Online] 2010. [Cited: February 26, 2012.] http://www.pveducation.org/pvcdrom/solar-cell-operation/solar-cell-structure.

[18]. Honsberg, Christiana and Bowden, Stuart, "Effect of Parasitic Resistances", PVEDUCATION, [Online] 2010. [Cited: February 26, 2012.] http://www.pveducation.org/pvcdrom/solar-cell-operation/effect-of-parasitic-resistances.

[19]. Messenger, Roger A. and Ventre, Jerry, *Photovoltaic Systems Engineering.* Florida : CRC Press LLC, 2005.

[20]. Honsberg, Christiana and Bowden, Stuart, "Short Circuit Current", PVEDUCATION, [Online] 2010. [Cited: February 26, 2012.] http://www.pveducation.org/pvcdrom/solar-cell-operation/short-circuit-current.

[21]. Honsberg, Christiana and Bowden, Stuart, "Short Circuit Current", PVEDUCATION, [Online] 2010. [Cited: July 24, 2011.] http://www.pveducation.org/pvcdrom/solar-cell-operation/short-circuit-current.

[22]. Sinton, R. A. and Cuevas, A., *Contactless determination of current–voltage characteristics and minority-carrier lifetimes in semiconductors from quasi-steady-state photoconductance data.* 1996, Applied Physics Letters, pp. 2510-2512.

[23]. Green, M. A., *Solar cell fill factors: General graph and empirical expressions.* 1981, Solid-State Electronics, pp. 788 - 789.

[24]. Honsberg, Christiana and Bowden, Stuart, "Efficiency" PVEDUCATION, [Online] 2010. [Cited: February 26, 2012.] http://www.pveducation.org/pvcdrom/solar-cell-operation/efficiency.

[25]. L. L. Kazmerski, "Best Research Cell Efficiency", [Online] 2011. [Cited: February 26, 2012.]

[26]. Honsberg, Christiana and Bowden, Stuart, "Series Resistance", PVEDUCATION, [Online] 2010. [Cited: July 24, 2011.] http://www.pveducation.org/pvcdrom/solar-cell-operation/series-resistance.

[27]. H. Lund, R. Nilsen, O. Salomatova, D. Skåre, E. Riisem**,** "Different Generations of Solar Cells", Solar Cells. [Online] 2008. [Cited: February 27, 2012.] http://org.ntnu.no/solarcells/pages/generations.php.

[28]. Queisser, William Shockley and Hans J.*,"* Detailed Balance Limit of Efficiency of p-n Junction Solar Cells" . 12, California : The American Institute of Physics, 1960, Vol. 32. ISSN.

[29]. Honsberg, Christiana and Bowden, Stuart, "Module Materials", PVEDUCATION, [Online] 2012. [Cited: February 29, 2012.] http://www.pveducation.org/pvcdrom/modules/module-materials.

[30]. Khan, B. H.*, Non Conventional Energy Technologies.* s.l. : McGrawHill, 2005.

[31]. Ayoub, Josef ;Bailey, Lisa Dignard ;Poissant, Yves, "National Reports", International Energy Agency Photovoltaic Power Systems Programme, [Online] 2010. [Cited: August 8, 2011.] http://www.iea-pvps.org/index.php?id=93&tx_damfrontend_pi1=&tx_damfrontend_pi1[catPlus]=&tx_damfrontend_pi1[catEquals]=&tx_damfrontend_pi1[catMinus]=&tx_damfrontend_pi1[catPlus_Rec]=71&tx_damfrontend_pi1[catMinus_Rec]=&tx_damfrontend_pi1[treeID]=201&tx_da.

[32]. U.S. Department of Energy, "Building Energy Software Tools Directory", Energy Efficiency and Renewable Energy, [Online] January 9, 2011. [Cited: July 30, 2011.]

http://apps1.eere.energy.gov/buildings/tools_directory/subjects.cfm/pagename=subjects/pagename_menu=other_applications/pagename=subjects#P.

[33]. PVRESOURCES**,** "Photovoltaic Software", PVRESOURCES, [Online] May 11, 2011. [Cited: July 30, 2011.] http://www.pvresources.com/en/software.php.

[34]. Homer Energy, "Optimizing Clean Power Everywhere", Homer Energy*,* [Online] [Cited: July 31, 2011.] http://www.homerenergy.com/index.html.

[35]. PVSYST SA, "PVSYST", Download PVSYST, [Online] [Cited: July 31, 2011.] http://www.pvsyst.com/.

[36]. Autodesk, "Autodesk Ecotect Ananlysis", Autodesk*,* [Online] [Cited: July 31, 2011.] http://usa.autodesk.com/adsk/servlet/download/item?siteID=123112&id=13140033.

[37]. Siraki, Arbi Gharakhani, Pillay, Pragasen and Williamson, Sheldon S.*,*"Comparison of PV System Design Software Packages for Urban Application", Montreal : World Energy Council, 2010. World Energy Congress, Montreal 2010.

[38]. Attia, Shady and Herde, André De., **"**Sizing Photovoltaic Systems during Early Design: A Decision Tool for Architects", Phoenix : American Solar Energy Society, 2010. SOLAR 2010.

[39]. Canadian Solar, "Products and Applications", Canadian Solar*,* [Online] [Cited: July 30, 2011.] http://www.canadiansolar.com/upload/modules/New%20Product%20Annoucement/New Edge%20All-black%20CS5A-MX_en.pdf.

[40]. Sharp, "Sharp NU Series", [Online] [Cited: July 30, 2011.] http://www.sharpdirect.co.uk/content/ebiz/sharp/resources/pdf/solarspecsheet_nu.pdf.

[41]. Ingeteam, "Photovoltaic Solar Energy", Ingeteam, [Online] [Cited: July 30, 2011.] http://www.ingeteam.it/userfiles/allegati/photovoltaicsolarenergyuk_1258046518.pdf.

[42]. Navigatuer Urban Software, "Navigatuer Urbain", [Online] [Cited: July 30, 2011.] www.navurb.com.

[43]. World, Maps of. Prevailing Winds, "Maps of World", [Online] [Cited: February 29, 2012.] http://www.mapsofworld.com/referrals/weather/weather-phenomenon/prevailing-winds.html.

[44]. Duffie, John A. and Beckman, William A., *Solar Engineering of Thermal Processes,* Wisconsin : John Wiley & Sons, 2006.

[45]. Nellis, Gregory and Klein, Sanford**,** *Heat Transer.* New York : Cambridge University Press, 2009.

[46]. McAdams, W. H., *Heat Transmission.* New York : McGraw-Hill, 1954.

[47]. Watmuff, J.H., Charter, W.W.S. and Proctor, D. , *Solar and wind induced external coefficients - Solar collectors.* 1977. Cooperation Mediterraneenne pour l'Energie Solaire, Revue Internationale d'Heliotechnique, 2nd Quarter. p. 56.

[48]. King, D. L.; Boyson, W. E.; Kratochvil, J. A., "Photovoltaic *Array Performance Model",* New Mexico : Sandia National Laboratories, 2004.

[49]. King, David L., Kratochvil, Jay A. and Boyson, William E. Anaheim, "Temperature Coefficient for PV Modules and Arrays : Measurement Methods, difficulties, and Results", CA : IEEE, 1997. 26th PVSC. pp. 1183-1186.

[50]. Oh, Jaewon and TamizhMani, GovindaSamy, "Temperature Testing and Analysis of PV Modules per ANSI/UL 1703 AND IEC 61730 Standards", Honolulu : IEEE, 2010. 35th IEEE Photovoltaic Specialists Conference. pp. 984-988.

[51]. TamizhMani, Govindasamy, "Photovoltaic Module Thermal/Wind Performance:Long -Term Monitoring and Model Development For Energy Rating", Colorado : National Renewable Energy Laboratory, 2003. NCPV and Solar Program Review Meeting 2003. pp. 936-939.

[52]. IEC, NOCT**,** *PV/61512 Testing and Measuring Equipment.* [Online] 2005. [Cited: July 28, 2011.] http://www.iecee.org/ctl/equipment/pdf/pv/EL_IEC61215_Ed1_final.pdf.

[53]. IEC. TC 82, *Solar photovoltaic energy systems*. *International Electrotechnical Commission.* [Online] October 2011. [Cited: July 28, 2011.] http://www.iec.ch/dyn/www/f?p=103:23:0::::FSP_ORG_ID:1276.

[54]. Green, M. A., "Solar Cells - Operating Principles, Technology and System Application", Kensington, Australia : University of NSW, 1992.

[55]. Koirala, Binod Prasad, Sahan, Benjamin and Henze, Norbert., "Study on MPP Mismatch Losses in Photovoltaic Applications", Hamburg : Fraunhofer, 2009. European Photovoltaic Solar Energy Conference and Exhibition (EU PVSEC). pp. 3727-3733.

[56]. Picault, D., "Changing photovoltaic array interconnections to reduce mismatch losses: a case study", Prague : EEEIC, 2010. International Conference on Environment and Electrical Engineering 2010.

[57]. Patel, Hiren and Agarwal, Vivek, *"MATLAB-Based Modeling to Study the Effects of Partial Shading on PV Array Characteristics",* IEEE Power and Energy Society, 2008. Energy Conversion. pp. 302-310.

Appendix

MATLAB Script

```
%Script for I-V Curve
%Abdul Adud, ID : 9756450
clear
clc
%PV cell parameters
Ic=2;
Is=10^-10;
q=1.6*10^-19;
k=1.38*10^-23;
T=300;
Vd=0:0.001:0.8;
Io=Ic-Is*(exp((q*Vd)/(k*T))-1);
% plotting PV cell output curve (output current Vs output Voltage)
plot(Vd,Io)
grid on;
title('Fig.1. I-V Characteristics of the PV cell')
xlabel('Vd (Volts)')
ylabel('Io (Amps)')
hold
Po=Vd.*Io;
plot(Vd,Po)
grid on;
title('Fig.2. Maximum Power Point of the cell')
xlabel('Vd (Volts)')
ylabel('Po (Watts)')
hold
max(Po)% provides the maximum value of cell power



% Script for Maximum Power Curve
% Abdul Adud ID : 9756450
Ic=2;
Is=10^-10;
q=1.6*10^-19;
k=1.38*10^-23;
T=300;
Vd=0:0.001:0.8;
Io=Ic-Is*(exp((q*Vd)/(k*T))-1);
Po=Vd.*Io;
plot(Vd,Po)
grid on;
title('Fig.2. Maximum Power Point of the cell')
xlabel('Vd (Volts)')
ylabel('Po (Watts)')
hold
max(Po)% provides the maximum value of cell power
```

```
% Script for Thermal Model
% Abdul Adud, ID : 9756450
q=1000; % Total flux
Dxg=.5*10^-2; % Glass Thickness
Dxi=10*10^-3;% Insulation thickness
x1=.03; % Air gap between plate and glass
x2=.25;% Insulation to ground clearance
Ka=.0275; % Conductivity Steven Boltzmann constant,of air
Ki=.045; % Conductivity of insulation
Kg=1;% Conductivity of glass
Eg=.88;% Emissivity of glass,
Ep=.88; % Emissivity of plate,
segma=5.67*10^-8; % Steven Boltzmann constant, ?
W=3; % Wind speed
Nu=5.572; %Nusselt constant for air
Ta=25+273; % ambient temperature
Ts=19+273; % sky temperature
% First of all we calculate all the known resistances
%back side
Ri=Dxi/Ki;
Rcia=x2/(Nu*Ka);
R_back=Ri+Rcia;
%front side
Rcpg=x1/(Nu*Ka); % Natural convection
Rp=Dxg/Kg;
Rcga=1/(5.7+(3.8*W)); % Forced convection
% now we assume the Tp and Tgh
Tp(1)=100+273;
Tgh(1)=50+273;
% now we calculate the fluxes in the front and in the back sides
q_back(1)=(Tp(1)-Ta)/R_back;
q_front(1)=q-(q_back(1));
% now the iterations
for (n=2:100000)
Rrpg(n)=1/((segma*((Tp(n-1)^2)+(Tgh(n-1)^2))*(Tp(n-1)+Tgh(n-
1)))/((1/Eg)+(1/Ep)-1);
Tgc(n-1)=Tgh(n-1)-(Rp*q_front(n-1));
Rrga(n)=1/(segma*Eg*((Tgc(n-1)^2)+(Ts^2))*(Tgc(n-1)+Ts));
R1(n)=(Rrpg(n)*Rcpg)/(Rrpg(n)+Rcpg);
R2(n)=((Rrga(n))*Rcga)/((Rrga(n))+Rcga);
R_front(n)=R1(n)+Rp+R2(n);
q_front(n)=(Tp(n-1)-Ta)/R_front(n);
q_back(n)=(Tp(n-1)-Ta)/R_back;
Tgh(n)=Tp(n-1)-(R1(n)*q_front(n));
Tgc(n)=Tgh(n)-(Rp*q_front(n));
if((q_front(n)+q_back(n))<q)
Tp(n)=Tp(n-1)+.01;
end
if((q_front(n)+q_back(n))>q)
Tp(n)=Tp(n-1)-.01;
end
end
T=Tp(n)-273
```